EFFECTS OF A TRANSIENT SEA SURFACE TEMPERATURE ANOMALY ON THE ENERGETICS OF THE MINTZ-ARAKAWA MODEL ATMOSPHERE

by

Shu-Hsien Chow

A Technical Report on research sponsored by the NASA Goddard Space Flight Center under Grant NGR 33-016-174 (to New York University) and Grant NGR 33-013-086 (to The City College of the City University of New York).

April 1974

Table of Contents

List of Figures

List of Figures(cont.)

Acknowledgements

The author is most grateful to her advisor, Professor Jerome Spar, for his advice and valuable suggestions throughout this work. She is also grateful to Professors Willard J. Pierson, Vincent Cardone and Raymond Deland for their advice and careful reading of this manuscript. Thanks are also due to Mr. John Liu, who furnished the history tapes of the transient SST anomaly experiment. In addition she wishes to thank her husband, Dr. Ming-Dah Chow, for his valuable discussions and encouragement.

This research was sponsored by the National Aeronautics and Space Administration, Goddard Space Flight Center, under Grants NGR 33-016-174 and NGR 33-013-086. Computing time was provided by the Goddard Institute for Space Studies (GISS). The author wishes to thank Dr. Robert Jastrow, Director, Dr. Milton Halem, and the Staff of GISS for their hospitality and services during the conduct of this research.

Abstract

The possible response of the atmosphere, as simulated by the two-level Mintz-Arakawa global general circulation model, to a transient (one month) North Pacific sea surface temperature (SST) anomaly is investigated in terms of the energetics both in the spatial and wave-number domains. In the first month, the increased heating, evaporation and condensation over the local anomaly region appear to cause an increase in the diabatic generation of eddy available potential energy in northern middle latitudes, and the increased temperature gradient, especially on the northern side of the warm pool, was found to increase the eddy conversion of the intermediate scales in northern middle latitudes. In the second month, on the other hand, the removal of the anomalous SST pattern appears to cause a reduction in eddy activity in northern middle latitudes, with the reduction taking place at all wave numbers. A large response to the transient North Pacific warm pool was also found in the southern middle latitudes during the second and third months. In general, the results indicate that the transient SST variations of reasonable magnitude in the North Pacific Ocean can induce a disturbing effect on the global energetics both in the spatial and wave-number domains.

The ability of the two-level Mintz-Arakawa model to simulate the atmospheric energetics is also examined in this study. Except in the tropics, the two-level Mintz-Arakawa model

exhibits a reasonable and realistic energy budget. One major defect of the model simulation is caused by the parameterization of convection, which produces too much convective precipitation in the tropics. The excessive convective precipitation in turn affects all the atmospheric energy transformation processes in the tropics.

1. Introduction

The prediction of weather anomalies and climatic fluctuations is a basic goal of meteorology. Several hypotheses have been proposed to account for anomalous weather and climate. For example, irregular variations of solar activity, variations in the proportion of atmospheric carbon dioxide, variations in the atmospheric turbidity resulting from intense volcanic eruptions, and abnormal surface boundary conditions such as sea ice, snow cover and sea surface temperature have all been proposed as important factors in weather and climatic variations. Some possible effects of sea surface temperature anomalies in the Pacific Ocean on the subsequent weather patterns were particularly studied by Namias (1963,1969,1971). Bjerknes (1966,1969) has also investigated the possible remote effects of anomalous sea surface temperature in the equatorial Pacific.

Recently, several computationally stable general circulation models have been developed (e.g., Mintz, 1965; Smagorinsky et al., 1965; Leith, 1967; Kasahara and Washington, 1967; Holloway and Manabe, 1971). These models provide the tools not only for learning the basic mechanisms of the general circulation and climatology of the atmosphere, but also for studying the possible responses of the atmosphere to various factors which may induce variations in weather and climate. Some experiments concerning the effects of sea surface temperature (SST) anomalies were carried out by Spar (1973,a,b,c)

with the two-level Mintz-Arakawa global general circulation model (Gates et al., 1971). Certain hypothetical anomalous patterns were superimposed on the Pacific SST field in those experiments. The imposed anomaly patterns persist either over a season or over one month. The responses of the model atmosphere to SST anomalies were discussed in terms of the monthly mean sea level pressure patterns and certain regional indices. The results showed that both transient and persistent SST anomalies produced significant responses in the hemisphere of the anomaly as well as in the opposite hemisphere.

The energetics of the atmosphere have been investigated intensively during the past few years. The purpose of studying the atmospheric energy budget is to reveal the basic mechanisms for maintaining the large-scale atmospheric circulation system. The basic nature of the atmospheric energetics may be changed due to climatic variations. For example, diagnostic studies of the kinetic energy exchange between zonal flow and large-scale eddies for the troposphere north of 20° N indicate the existence of an unusual type of circulation in January 1963 (Wiin-Nielsen, Brown and Drake, 1964; Murakami and Tomatsu, 1965; Brown, 1967). Studies for that month indicate that kinetic energy was transformed from zonal to eddy form during this winter period, whereas this exchange mechanism is usually in the opposite direction (e.g., Oort, 1964; Saltzman, 1970). According to Namias (1963), positive SST anomalies in the central and eastern North Pacific Ocean were fairly per-

sistent during the last half of 1962 and early 1963. The case of January 1963 seems to suggest that SST anomalies may produce significant effects on the atmospheric energetics.[1] The fact that the sea level pressure fields exhibited world-wide responses to the SST anomalies (Spar,1973a, 1973c) seems to indicate that the SST anomalies might induce world-wide effects on the atmospheric energetics.

The purpose of this study is to investigate the response of the atmosphere to certain SST anomalies from the energetics point of view. The case of the transient (one month) SST anomaly (Spar, 1973c) was chosen for detailed analysis. In this experiment, the anomalous warm pool was located in the North Pacific Ocean, in an area bounded by 22°N - 42°N and 140°W - 180°W, and persisted over a period of only one month. In the first month, two effects of the SST anomaly are expected to affect the atmospheric energetics. One is the augmented heating, evaporation, and condensation over the local anomaly region, which is expected to increase the diabatic generation of eddy available potential energy. The other is the increased temperature gradient, especially on the northern side of the warm pool. According to the baroclinic instability theory (e.g., Charney,1947), the increased temperature gradient is favorable for baroclinic instability.

---

[1] However, it must be noted that we do not expect the similar effects of January 1963 to appear in the analysis of this study. This is because that the pattern and duration of SST anomaly and the initial condition of the transient SST anomaly experiment (Spar, 1973c) are different from those of January 1963.

Since the conversion of eddy available potential energy to eddy kinetic energy is responsible for the growth of the disturbance in a baroclinic atmosphere (e.g., Brown, 1969), this conversion is also expected to increase, especially for the most unstable waves. On the other hand, in the second month the removal of the SST anomaly is expected to reduce condensation and produce a cooling effect over the warm pool region. In this study, the propagation of these effects and the influence on the other energy transformation processes are investigated. The results are discussed in section 7.

In order to evaluate the significance of such a simulation of climate modification due to SST anomalies, it is necessary to assess the ability of the model to simulate the real atmosphere. A comparison of the energetics of the model "control run", which was designed to simulate the "normal" atmosphere, with no SST anomaly, with the "observed" atmosphere is presented in section 6.

The energy equations integrated over the entire global atmosphere have been derived by Lorenz(1955) and Saltzman(1957). Since then atmospheric energetics have been computed extensively based on these equations. Because this study is concerned primarily with the possible effects of SST anomalies on different parts of the atmosphere, spectral energy equations for latitude belts instead of the global integrated energy equations were used. Following the approaches of Lorenz(1955) and Saltzman(1957), the energy equations for

a latitude belt both in the spatial and wave-number domains were derived, and are presented in sections 2 and3. The model energetics were computed from the daily mean values of the Fourier representations of variables defined at isobaric surface, and the harmonics were calculated up to wave number 15, based on information at 72 points around a latitude circle.

2. Formulations in the spatial domain

2.1. Fundamental equations in the spatial domain

By adopting the hydrostatic approximation, the governing fundamental equations (i.e., the equations of motion, thermodynamic energy, and continuity) in the (λ, ϕ, p, t) coordinate system may be written as follows:

$$u_t + \frac{u}{a\cos\phi}\,u_\lambda + \frac{v}{a}\,u_\phi + \omega u_p - \left(f + \frac{u\tan\phi}{a}\right)v + \frac{1}{a\cos\phi}\,\Phi_\lambda + x = o \tag{2.1}$$

$$v_t + \frac{u}{a\cos\phi}\,v_\lambda + \frac{v}{a}\,v_\phi + \omega v_p + \left(f + \frac{u\tan\phi}{a}\right)u + \frac{1}{a}\,\Phi_\phi + y = o \tag{2.2}$$

$$\Phi_p + \frac{RT}{p} = o \tag{2.3}$$

$$\omega_p + \frac{1}{a\cos\phi}\,(u_\lambda + (v\cos\phi)_\phi) = o \tag{2.4}$$

$$T_t + \frac{u}{a\cos\phi}\,T_\lambda + \frac{v}{a}\,T_\phi + \omega T_p - \frac{R}{c_p p}\,\omega T - \frac{h}{c_p} = o \tag{2.5}$$

in which

t = time,

λ = longitude,

ϕ = latitude,

p = pressure,

a = radius of the earth,

$u = a\cos\phi\, d\lambda/dt$, eastward wind speed,

v = $a\, d\phi/dt$, northward wind speed,

ω = dp/dt, vertical p-velocity,

Φ = geopotential,

T = temperature,

$\dot{h}$ = diabatic heating rate,

g = acceleration of gravity,

R = gas constant for air,

c_p = specific heat at constant pressure,

f = Coriolis parameter,

x = eastward component of frictional force,

y = northward component of frictional force.

2.2. Energy equations in the spatial domain

The total potential energy of the atmosphere, which is the sum of potential and internal energies, is the only source for the kinetic energy of the whole atmosphere. However, it is not a good measure of the amount of energy available for conversion to kinetic energy. For a horizontally stratified and stable atmosphere, although total potential energy is plentiful, none at all is available for conversion to kinetic energy. Thus, in his discussion of the atmospheric energy cycle, Lorenz (1955) defined the available potential energy of the atmosphere as the difference between the total potential energy of the whole atmosphere and the total potential energy which would exist under any adiabatic redistribution of mass to yield a horizontal stable stratification.

This concept was also discussed by Margules (1903) in his famous paper concerning the energy of storms.

The available potential energy was formulated by Lorenz (1955) for isobaric surfaces. Based on this formulation, the available potential energy has been computed extensively in observational studies. Modifications of Lorenz's (1955) definition of available potential energy have been proposed (e.g., Van Mieghem, 1956; Dutton and Johnson, 1967). In this study, Lorenz's (1955) approach is adopted to make the energetics of the model atmosphere comparable to observations.

Let K and P be the kinetic and available potential energies per unit mass, respectively, which are defined as

$$K \equiv (u^2 + v^2)/2 \quad ,$$

$$P \equiv c_p \gamma T''^2/2 \quad ,$$

where $(\ )''$ denotes the deviation from area average over an isobaric surface, $\tilde{(\ )}$, and γ (see Saltzman, 1957) is given as

$$\gamma \equiv \left(\tilde{T} - \frac{c_p p}{R} \tilde{T}_p \right)^{-1} \quad .$$

Let [ ] denote the zonal average, defined as

$$[b] \equiv \frac{1}{2\pi} \int_0^{2\pi} b \, d\lambda \quad ,$$

and let $(\ )^*$ denote the deviation from the zonal average, [ ]. Then the kinetic and available potential energies may be decomposed into zonal and eddy components, as follows,

$$K = K_z + K_E \quad ,$$

$$P = P_z + P_E \quad ,$$

where

$$K_z = ([u]^2 + [v]^2)/2 \quad ,$$

$$K_E = ([u]\, u^* + [v]\, v^*) + (u^{*2} + v^{*2})/2 \quad ,$$

$$P_z = c_p \gamma [T]''^2/2 \quad ,$$

$$P_E = c_p \gamma [T]'' T^* + c_p \gamma T^{*2}/2 \quad ,$$

K_z and K_E are the zonal and eddy kinetic energy per unit mass, respectively; P_z and P_E are the zonal and eddy available potential energy per unit mass, respectively.

The energy equations per unit mass over a latitude belt, derived from the fundamental equations (2.1)-(2.5), may be written as

$$(K_z)_t = F(K_z) - \langle K_z, K_E \rangle + \langle P_z, K_z \rangle + W_z + D_z \quad , \tag{2.6}$$

$$[K_E]_t = F(K_E) + \langle K_z, K_E \rangle + \langle P_E, K_E \rangle + W_E + D_E \quad , \tag{2.7}$$

$$(P_z)_t = F(P_z) - \langle P_z, P_E \rangle - \langle P_z, K_z \rangle + G_z + CRZ \quad , \tag{2.8}$$

$$[P_E]_t = F(P_E) + \langle P_z, P_E \rangle - \langle P_E, K_E \rangle + G_E + CRE \quad , \tag{2.9}$$

where

$$F(K_z) = F_1(K_z) + F_2(K_z) \quad ,$$

$$F_1(K_z) = - \left\{ \frac{1}{a \cos \phi} ([v K_z] \cos \phi)_\phi + [\omega K_z]_p \right\} \quad ,$$

$$F_2(K_z) = - \frac{1}{a \cos \phi} \left\{ ([u][u^* v^*] + [v][v^{*2}]) \cos \phi \right\}_\phi - \left\{ [u][\omega^* u^*] + [v][v^* \omega^*] \right\}_p \quad ,$$

$$F(K_E) = F_1(K_E) + F_2(K_E) \quad ,$$

$$F_1(K_E) = - \left\{ \frac{1}{a \cos \phi} ([v K_E] \cos \phi)_\phi + [\omega K_E]_p \right\} \quad ,$$

$$F_2(K_E) = - F_2(K_z) \quad ,$$

$$F(P_z) = F_1(P_z) + F_2(P_z) \quad ,$$

$$F_1(P_z) = - \left\{ \frac{1}{a \cos \phi} ([v P_z] \cos \phi)_\phi + \gamma ([\omega P_z]/\gamma)_p \right\} \quad ,$$

$$F_2(P_z) = - c_p \gamma \left\{ \frac{1}{a \cos \phi} ([T]'' [v^* T^*] \cos \phi)_\phi + ([T]'' [\omega^* T^*])_p \right\} \quad ,$$

$$F(P_E) = F_1(P_E) + F_2(P_E) \quad ,$$

$$F_1(P_E) = -\left\{ \frac{1}{a \cos\phi} \left([v\, P_E] \cos\phi\right)_\phi + \gamma \left([\omega\, P_E]/\gamma\right)_p \right\} \quad ,$$

$$F_2(P_E) = -\, F_2(P_Z) \quad ,$$

$$\langle K_z, K_E \rangle = -\left\{ [u^* v^*] \frac{\cos\phi}{a} \left([u]/\cos\phi\right)_\phi + \frac{[v^{*2}]}{a} [v]_\phi + [\omega^* u^*] [u]_p \right.$$

$$\left. + [\omega^* v^*] [v]_p - [u^{*2}] [v] \frac{\tan\phi}{a} \right\} \quad ,$$

$$\langle P_z, P_E \rangle = -\, c_p \gamma \left\{ \frac{1}{a \cos\phi} [v^* T^*] [T]_\phi + [\omega^* T^*] \left([T]_p'' - \frac{R}{c_p P} [T]'' \right) \right\} \quad ,$$

$$\langle P_z, K_z \rangle = -\, \frac{R}{p} [\omega] [T]'' \quad ,$$

$$\langle P_E, K_E \rangle = -\, \frac{R}{p} [\omega^* T^*] \quad ,$$

$$W_z = -\left\{ \frac{1}{a \cos\phi} \left([v] [\Phi]'' \cos\phi\right)_\phi + \left([\omega] [\Phi]''\right)_p \right\} \quad ,$$

$$W_E = -\left\{ \frac{1}{a \cos\phi} \left([v^* \Phi^*] \cos\phi\right)_\phi + [\omega^* \Phi^*]_p \right\} \quad ,$$

$$D_z = -[u] [x] - [v] [y] \quad ,$$

$$D_E = -[u^* x^*] - [v^* y^*] \quad ,$$

$$G_z = \gamma [h] [T]'' \quad ,$$

$$G_E = \gamma [h^* T^*] \quad ,$$

$$CRZ = \left([\omega\, P_z] + c_p \gamma [T]'' [\omega^* T^*] \right) \frac{2R}{c_p p} \quad ,$$

$$CRE = \left([\omega P_E] - c_p \gamma [T]'' [\omega^* T^*] \right) \frac{2R}{c_p p} \quad ,$$

$F(b)$ represents the flux convergence of b; $\langle b_1, b_2 \rangle$ represents the conversion from b_1 to b_2 ($\langle b_1, b_2 \rangle = - \langle b_2, b_1 \rangle$); W_Z and W_E are the energy exchanges with surroundings through zonal and eddy pressure interactions, respectively; D_Z and D_E are the frictional dissipations of zonal and eddy kinetic energy, respectively; G_Z and G_E are the generations of zonal and eddy available potential energy, respectively, by diabatic heating. CRZ and CRE are the extra terms which arise from the simplified definition of available potential energy. These two terms, which were neglected in the global integrated energy equations (e.g., Saltzman, 1957), are disregarded in the following discussion. Note that for the area north of 20°N, the neglect of CRZ and CRE will not make the model computation inconsistent with the observations.

Eqs. (2.6) - (2.9) are used to compute the energetics for latitude belts. These equations integrated over the entire mass of the atmosphere are essentially the same as those derived by other investigators (e.g., Lorenz, 1955; Saltzman, 1957; Oort, 1964), and can be used to estimate the energy cycle for the entire atmosphere. Note that the definitions of $\langle P_Z, K_Z \rangle$ and G_Z in this study are different from those generally used (see Lorenz, 1955; Saltzman, 1957). For example, $\langle P_Z, K_Z \rangle$ and G_Z were defined by Saltzman (1957) as $\frac{R}{p} [\omega]'' [T]''$ and $\gamma [h]'' [T]''$, respectively. The flux convergence terms ($F(K_Z)$, $F(K_E)$, $F(P_Z)$ and $F(P_E)$) and pressure interaction terms (W_Z and W_E) are disregarded in the global integrated energy equations. However, these terms

cannot be disregarded in the energy budget for a latitude belt. The other transformation terms in this paper are essentially the same as those generally defined.

3. Formulations in the wave-number domain

3.1 Fundamental equations in the wave-number domain

Let $\zeta(\lambda)$ and $Z(n)$ be the Fourier transform pair defined as follows:

$$\zeta(\lambda) = \sum_{n=-\infty}^{\infty} Z(n)\, e^{in\lambda} \quad , \tag{3.1}$$

and

$$Z(n) = \frac{1}{2\pi} \int_{0}^{2\pi} \zeta(\lambda)\, e^{-in\lambda}\, d\lambda \quad . \tag{3.2}$$

The Fourier transform pairs to be considered in this study are listed in Table 1.

Table 1. Fourier transform pairs

$\zeta(\lambda)$	u	v	ω	ϕ	T	h	x	y
$Z(n)$	U	V	Ω	A	B	H	X	Y

By multiplying Eqs. (2.1) - (2.5) by $(2\pi)^{-1} e^{-in\lambda}$, and integrating around a latitude circle, the spectral forms of the fundamental equations can be obtained (Saltzman, 1957). The spectral equations of horizontal motion may be written as

$$(U(n))_t = - \sum_{m=-\infty}^{\infty} \left\{ \frac{im}{a \cos\phi} U(m)\, U(n-m) + \frac{1}{a} U_\phi(m)\, V(n-m) \right.$$

$$\left. + U_p(m)\,\Omega(n-m) - \frac{\tan\phi}{a} U(m)\, V(n-m) \right\} \qquad (3.3)$$

$$- \frac{in}{a \cos\phi} A(n) + f\, V(n) - X(n) \quad ,$$

and

$$(V(n))_t = - \sum_{m=-\infty}^{\infty} \left\{ \frac{im}{a \cos\phi} V(m)\, U(n-m) + \frac{1}{a} V_\phi(m)\, V(n-m) \right.$$

$$\left. + V_p(m)\,\Omega(n-m) + \frac{\tan\phi}{a} U(m)\, U(n-m) \right\} \qquad (3.4)$$

$$- \frac{1}{a} A_\phi(n) - f\, U(n) - Y(n) \quad .$$

where m and n are the wave numbers around a latitude circle. The spectral hydrostatic equation may be written as

$$A_p(n) = - \frac{R}{p} B(n) \quad . \qquad (3.5)$$

The spectral equation of continuity may be written as

$$\Omega_p(n) = - \left\{ \frac{in}{a \cos\phi} U(n) + \frac{1}{a} V_\phi(n) - \frac{\tan\phi}{a} V(n) \right\} \quad . \qquad (3.6)$$

The spectral thermodynamic energy equation may be written as

$$(B(n))_t = -\sum_{m=-\infty}^{\infty} \left\{ \frac{im}{a\cos\phi} B(m)\, U(n-m) + \frac{1}{a} B_\phi(m)\, V(n-m) \right.$$

$$\left. + B_p(m)\,\Omega(n-m) - \frac{R}{c_p p} B(m)\,\Omega(n-m) \right\} \qquad (3.7)$$

$$+ \frac{1}{c_p} H(n) \quad .$$

3.2 Energy equations in the wave-number domain

If $Z(n)$ and $Q(n)$ are the Fourier transforms of $\zeta(\lambda)$ and $q(\lambda)$, respectively, the Parseval theorem may be written as

$$2\pi \int_0^{2\pi} \zeta(\lambda)\, q(\lambda)\, d\lambda = \sum_{m=-\infty}^{\infty} Q(m)\, Z(-m) \quad . \qquad (3.8)$$

By means of Parseval theorem, zonal averages of kinetic and available potential energies can be expressed as

$$[K] = \tfrac{1}{2}\left([u]^2 + [v]^2\right) + \sum_{n=1}^{\infty} \left(|U(n)|^2 + |V(n)|^2\right) \quad ,$$

and

$$[P] = \tfrac{1}{2} c_p \gamma [T]^2 + \sum_{n=1}^{\infty} c_p \gamma |B(n)|^2 \quad .$$

If we define

$$K(n) = |U(n)|^2 + |V(n)|^2 \quad ,$$

$$P(n) = c_p \gamma |B(n)|^2 \quad ,$$

then [K] and [P] can be expressed as

$$[K] = K_z + \sum_{n=1}^{\infty} K(n) \quad ,$$

$$[P] = P_z + \sum_{n=1}^{\infty} P(n) \quad ,$$

where $K(n)$ is the eddy kinetic energy of the nth component per unit mass in a latitude belt, and $P(n)$ is the eddy available potential energy of the nth component per unit mass in a latitude belt. Note that $K_E = \sum_{n=1}^{\infty} K(n)$, and $P_E = \sum_{n=1}^{\infty} P(n)$.

Saltzman (1957) derived the spectral energy equations for the entire atmosphere. However, as mentioned before, in order to be able to see the effects of SST anomalies on different parts of the atmosphere, the calculations were based on the spectral energy equations for a latitude belt.

After multiplying Eqs. (3.3) and (3.4) by $U(-n)$ and $V(-n)$, respectively, and the equations for $(U(-n))_t$ and $(V(-n))_t$ by $U(n)$ and $V(n)$, respectively, the eddy

kinetic energy equation for the nth component can be obtained by adding the resulting four equations (see Saltzman, 1957). Similarly, multiplying Eq. (3.7) by $B(-n)$ and the equation for $(B(-n))_t$ by $B(n)$, respectively, the eddy available potential energy equation for the nth component can be obtained by adding the resulting two equations. These spectral energy equations for a latitude belt may be written as

$$(K(n))_t = F(K(n)) + M(n) + L(n) + C(n) + W(n) + D(n) \quad , \tag{3.9}$$

$$(P(n))_t = F(P(n)) + Q(n) + S(n) - C(n) + G(n) \quad , \tag{3.10}$$

where

$$F(K(n)) = - \sum_{\substack{m=-\infty \\ \neq o}}^{\infty} \left\{ \frac{1}{a \cos\phi} \left(\left(\frac{U(m)}{2} \psi_{vu}(m,n) + \frac{V(m)}{2} \psi_{vv}(m,n) \right) \cos\phi \right)_{\phi} \right.$$

$$\left. + \left(\frac{U(m)}{2} \psi_{\omega u}(m,n) + \frac{V(m)}{2} \psi_{\omega v}(m,n) \right)_p \right\} \quad ,$$

$$F(P(n)) = - \sum_{\substack{m=-\infty \\ \neq o}}^{\infty} c_p \gamma \left\{ \frac{1}{a \cos\phi} \left(\frac{B(m)}{2} \psi_{vT}(m,n) \cos\phi \right)_{\phi} \right.$$

$$\left. + \left(\frac{B(m)}{2} \psi_{\omega T}(m,n) \right)_p \right\} \quad ,$$

$$M(n) = -\left\{ \chi_{uv}(n) \frac{\cos\phi}{a} \left([u]/\cos\phi\right)_{\phi} + \chi_{vv}(n) \frac{1}{a} [v]_{\phi} \right.$$

$$\left. + \chi_{u\omega}(n) [u]_p + \chi_{v\omega}(n) [v]_p - \chi_{uu}(n) [v] \frac{\tan\phi}{a} \right\} ,$$

$$Q(n) = -c_p \gamma \left\{ \frac{1}{a} \chi_{vT}(n) [T]_{\phi} + \chi_{\omega T}(n) \left([T]''_p - \frac{R}{c_{pp}} [T]'' \right) \right\} ,$$

$$L(n) = L_1(n) + L_2(n)$$

$$L_1(n) = \sum_{\substack{m=-\infty \\ \neq 0}}^{\infty} \left\{ U(m) \left(\frac{1}{a\cos\phi} \psi_{uu_{\lambda}}(m,n) + \frac{1}{a} \psi_{vu_{\phi}}(m,n) \right.\right.$$

$$\left. + \psi_{\omega u_p}(m,n) - \frac{\tan\phi}{a} \psi_{uv}(m,n) \right) + V(m) \left(\frac{1}{a\cos\phi} \psi_{uv_{\lambda}}(m,n) \right.$$

$$\left.\left. + \frac{1}{a} \psi_{vv_{\phi}}(m,n) + \psi_{\omega v_p}(m,n) + \frac{\tan\phi}{a} \psi_{uu}(m,n) \right) \right\} ,$$

$$L_2(n) = F(K(n)) ,$$

$$S(n) = S_1(n) + S_2(n) ,$$

$$S_1(n) = \sum_{\substack{m=-\infty \\ \neq 0}}^{\infty} c_p \gamma B(m) \left\{ \frac{1}{a\cos\phi} \psi_{uT_{\lambda}}(m,n) + \frac{1}{a} \psi_{vT_{\phi}}(m,n) \right.$$

$$\left. + \psi_{\omega T_p}(m,n) \right\} ,$$

$$S_2(n) = F(P(n)) \quad ,$$

$$C(n) = -\frac{R}{P}\chi_{\omega T}(n) \quad ,$$

$$W(n) \doteq -\left\{\frac{1}{a\cos\varphi}\left(\chi_{v\Phi}(n)\cos\phi\right)_{\phi} + \left(\chi_{\omega\Phi}(n)\right)_p\right\} \quad ,$$

$$D(n) = -\chi_{ux}(n) - \chi_{vy}(n) \quad ,$$

$$G(n) = \gamma\,\chi_{Th}(n) \quad ,$$

in which[2]

$$\chi_{\zeta q}(n) = [\,Z(n)\,Q(-n) + Z(-n)\,Q(n)\,] \quad ,$$

$$\psi_{\zeta q}(m,n) = [\,Z(n-m)\,Q(-n) + Z(-n-m)\,Q(n)\,] \quad ,$$

with $Z(n)$ and $Q(n)$ being the Fourier transforms of $\zeta(\lambda)$ and $q(\lambda)$, respectively. $F(K(n))$ is the flux convergence of eddy kinetic energy of the nth component; $F(P(n))$ is the flux convergence of eddy available potential energy of the nth component; $M(n)$ is the transfer from zonal kinetic energy to eddy kinetic energy of the nth component; $Q(n)$ is the transfer from zonal available potential energy to eddy available potential

---

[2] It may be verified from Parseval theorem (3.8) that $[\zeta^*(\lambda)\,q^*(\lambda)] = \sum_{n=1}^{\infty}\chi_{\zeta q}(n)$.

It may also be verified from the definitions of Fourier transform (3.1) and (3.2) that $[u^*(\lambda)\,q^*(\lambda)\,\zeta(\lambda)] = \sum_{n=1}^{\infty}\sum_{\substack{m=-\infty \\ \neq 0}}^{\infty} U(m)\,\psi_{\zeta q}(m,n)$.

energy of the nth component; $L(n)$ is the kinetic energy transfer from other wave components to the nth component through nonlinear wave interations; $S(n)$ is the available potential energy transfer from other wave components to the nth component through nonlinear wave interations; $C(n)$ is the eddy conversion from available potential energy to kinetic energy for the nth component; $W(n)$ is the energy exchange with the surroundings through eddy pressure interation of the nth component; $D(n)$ is the frictional dissipation of eddy kinetic energy of the nth component; $G(n)$ is the generation of eddy available potential energy of the nth component.

Eqs. (3.9) and (3.10) are used to compute the spectral energetics for latitude belts. These two equations together with Eqs. (2.6) and (2.8) integrated over the entire mass of the atmosphere are essentially the same as those derived by Saltzman (1957), and can be used to estimate the energy cycle for the whole atmosphere in the wave-number domain.

The relationships between the energy transformation terms in the spatial domain and those in the wave-number domain are given in Table 2.

Table 2. Relationships of energy transformations between spatial domain and wave-number domain

spatial domain	wave-number domain
$F(K_E)$	$\sum_{n=1}^{M2} F(K(n))$
$F(P_E)$	$\sum_{n=1}^{M2} F(P(n))$
$\langle K_Z, K_E \rangle$	$\sum_{n=1}^{M2} M(n)$
$\langle P_Z, P_E \rangle$	$\sum_{n=1}^{M2} Q(n)$
$\langle P_E, K_E \rangle$	$\sum_{n=1}^{M2} C(n)$
W_E	$\sum_{n=1}^{M1} W(n)$
D_E	$\sum_{n=1}^{M2} D(n)$
G_E	$\sum_{n=1}^{M2} G(n)$
0	$\sum_{n=1}^{M2} L(n)$
CRE (=0)[3]	$\sum_{n=1}^{M2} S(n)$

[3] CRE is neglected in this study.

4. Brief descriptions of the general circulation model and the transient SST anomaly experiment

A transient SST anomaly experiment was carried out by Spar (1973c) with the two-level Mintz-Arakawa global general circulation model. The details of the model structure are described by Gates et al. (1971). A very brief description of the model and the experiment is given below.

The model is a two-layer global tropospheric model, and is bounded by the earth's surface and the 200 mb level. The primitive equations are solved on a spherical grid of 5° of longitude by 4° of latitude. The large-scale mountain system is incorporated by using σ-coordinate. ($\sigma = (p - p_T)/(p_s - p_T)$, where p_T is the pressure of the tropopause and is taken to be 200 mb, and p_s is the pressure of earth's surface). Land and sea distributions are also included in the model. Temperatures of land are determined from a surface energy balance condition. Sea surface temperatures are prescribed as the climatological annual mean values. The model also includes a water cycle (with clouds and precipitation), parameterization of convection, radiation (including continuously varying solar distance, declination and zenith angle) (Arakawa et al., 1968), and a prescribed seasonal variation in the latitude of the northern hemisphere snow line.

In the transient SST anomaly experiment, the anomalous warm pool was chosen to locate in the North Pacific Ocean, in an area bounded by $22^{\circ}N$-$42^{\circ}N$ and $140^{\circ}W$-$180^{\circ}W$.

An anomalous pattern from 2°C to 6°C was added to the climatological mean annual sea surface temperature of this area. The anomaly on the perimeter grid points of this area was set at 2°C, increasing to 4°C at points one gridpoint in from the perimeter, and to a maximum of 6°C at points two gridpoints in from the perimeter. The warm oceanic pool was allowed to persist for the first month of the anomaly run, after which time the climatological mean annual SST pattern was restored. The simulated predictions were carried out for 90 forcast days of the winter season.

5. Methods of calculations

History tapes of the experiment with the transient SST anomaly (Spar, 1973c) obtained from the two-layer Mintz-Arakawa global general circulation model were used. The general circulation model was designed to simulate the troposphere, which was assumed to be bounded between 200 mb and the earth's surface. In the computation of energetics, since the p-coordinate was used, the lower boundary was assumed to be the 1000 mb surface instead of the earth's surface. The troposphere was also divided into two layers with the 600 mb surface being the interface.

Variables on an isobaric surface were interpolated from data of history tapes which were computed in σ coordinates. Horizontal velocities and frictional forces were interpolated linearly in σ-space. In the interpolations of temperatures, geopotentials and temperature lapse rates, it was assumed, as in the general circulation model, that the potential temperature was linear in $(p)^{R/c_p}$ space. For the vertical p-velocities, a parabolic profile in σ-space was adopted.

The diabatic heating includes solar radiation, long-wave radiation, condensation and the surface sensible heat exchange. The condensation is due to both large-scale and convective processes. In order to examine the role of various heating components in the generation of available potential energy, these heating components were separated. In the general circulation model, the large-scale condensation and the

surface sensible heat exchange were assumed to occur only in the lower layer and were defined on the $\sigma=3/4$ surface. These two heating components were then assumed to be the heating components on the 800 mb surface for computing the energetics. The rest of the heating components on the 400 mb and 800 mb were interpolated linearly in σ-space.

As in the general circulation model, horizonal velocities and frictional forces were defined at latitudes from 88°S to 88°N with 4° interval, and the rest of the variables were defined from 90°S to 90°N with 4° interval. The Fourier components of the variables on the isobaric surfaces were computed up to wave number 15. The energetics were then computed at latitudes from 86°S to 86°N with 4° interval using daily mean values of the Fourier components of the variables. In calculating the budget of available potential energy, the value of γ used was the mean value of the stability factor over 90 days.

The summation of L(n) and that of S(n) over 15 wave numbers are in general not equal to zero. This is because of the truncation in wave number, of the finite differences employed in calculating the values of derivatives of variables, and of the nonzero of the CRE. The nonzero sums were assumed to be uniformly distributed over all waves. The corrected L(n) was set to be equal to L(n) defined in section 3 minus a correction which is the summation of L(n) over all waves devided by the number of waves. The same approximation

was also adopted earlier by Saltzman and Fleisher (1960) and Yang (1967).

The energetics integrated through the entire depth of the model atmosphere were computed. Since the vertical p-velocities were assumed to be zero at 200 mb surface, integrating the divergences of vertical transport terms ($(\omega K_z)_p$, $(\omega K_E)_p$, etc.) yields the vertical transports at the lower boundary. In order to incorporate the topographic effect, this lower boundary was set to be the earth's surface rather than the 1000 mb surface. Six pressure surfaces, i.e., 700, 800, 850,900,950 and 1000 mb, were chosen to represent the lower boundary for different grid points in calculating the vertical transports of available potential energy and geopotential deviations near the earth's surface. If the earth's elevation at a grid point is higher than the height of 775 mb in the NACA standard atmosphere, the lower boundary for that grid point was set at 700 mb. If it is lower than the standard height of 975 mb, 1000 mb was chosen to be the lower boundary for that grid point.

6. Energetics of the model atmosphere

6.1. Energetics of the control run in the spatial domain for the region north of 20°N

Before investigating the possible effects of a transient SST anomaly on the atmospheric energetics, it is desirable to examine how well the model atmosphere simulates the real atmospheric processes and energy contents. Since the general circulation of the control run was designed to simulate normal climate, the energetics of the control run are compared with the observations.

The energetics of the atmosphere have been computed intensively based on observed data. However, most of the observational studies are confined to the Northern Hemisphere, especially to the region north of 20°N (see Oort,1964; Krueger et al., 1965; Saltzman, 1970; etc). Since the energetics might be quite different over different parts of the atmosphere, only the results for the control run north of 20°N are compared with the observations.

Fig. 1 shows the ninety-day mean energy budget in the spatial domain for the winter control run averaged over the area north of 20°N, together with observational results from Krueger et al. (1965) and Saltzman (1970). The energy estimates by Krueger et al. (1965) shown in Fig. 1 are for an average of 5 winter (December- February) seasons, and are based on data from 850 mb to 500 mb in the region north of 20°N, extrapolated to include the entire atmosphere. Based

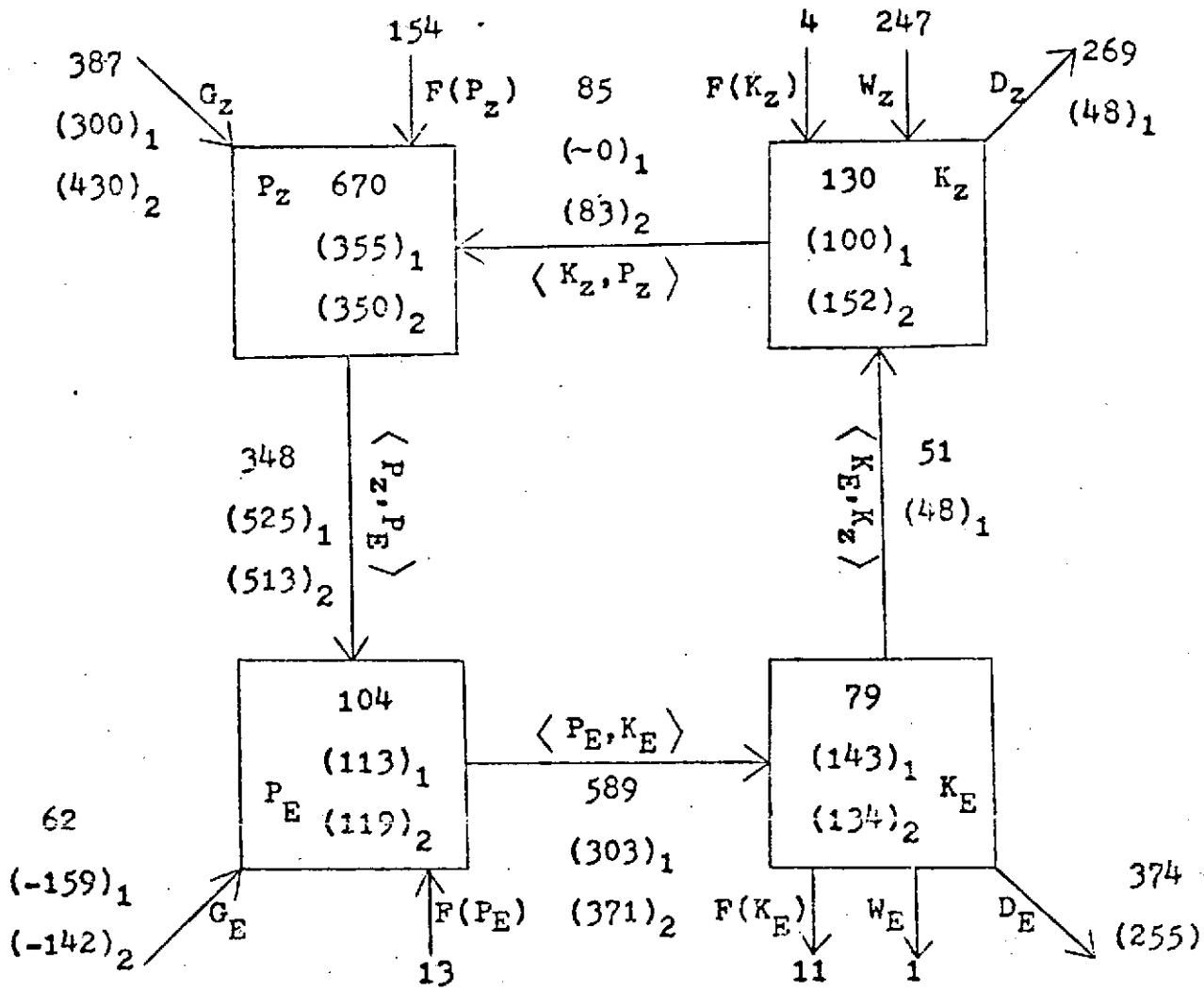

Fig. 1. The ninety-day mean energy budget in the spatial domain for winter control run averaged over area north of 20°N.

on a variety of sources, Saltzman (1970) compiled a spectral energy budget for the Northern Hemisphere. His results for an average "cold season", October - March, transformed into the spatial domain, are also shown in Fig. 1 for comparison.

In general, the so-called observational energetics of the atmosphere have been estimated (e.g., Oort, 1964; Saltzman, 1970) by applying the global integrated energy equations to the data in certain latitude bands within the Northern Hemisphere (approximately north of 20^{o}N or 15^{o}N). The model energetics, on the other hand, were computed from the zonal averaged energy equations for all latitude bands covering the entire global atmosphere below 200 mb. The region north of 20^{o}N is an open domain in the model calculations, therefore, the model energetics include the energy flux convergence and pressure interaction terms, which were neglected in the observational studies. According to Fig.1, the convergence of zonal available potential energy, $F(P_z)$, and the zonal pressure interaction, W_z, play an important role in the energy budget of this region.

The zonal available potential energy, P_z , of the winter control run appears to be too large compared with the observations. One reason for this discrepancy is the difference of domains between the model and observational computations. Squares of the temperature deviations from the global mean temperature were used to compute P_z in the model energetics, while deviations from the limited area mean temperature

(e.g., north of 20°N) were used in the observational studies. Another reason is that the model produces excessively high temperature in the upper troposphere in the tropics. In the January climate simulation, Gates (1972) also found that the temperatures in the upper level of the tropics were much higher than those observed. This is because the model produces too much convective precipitation in the tropics.

The zonal kinetic energy, K_Z, of the model control run is in good agreement with the observations, and so is the eddy available potential energy, P_E. On the other hand, the eddy kinetic energy, K_E, calculated from the model is too small, probably as a result of the low horizontal resolution of the model. Both Manabe et al. (1970) and Wellck et al. (1971) found that the eddy kinetic energy was markedly increased by increasing the horizontal resolution of the model.

The zonal conversion $\langle P_Z, K_Z \rangle$ indicates a conversion from zonal kinetic to zonal potential energy in the model north of 20°N, in good agreement with the result of Krueger et al. (1965). The negative of this conversion reflects the dominance of the indirect cell north of 20°N. On the other hand, the eddy conversion, $\langle P_E, K_E \rangle$, from eddy available potential to eddy kinetic energy, appears to be too large in the model compared with the observations. However, this conversion was computed from the vertical motion field, which was determined dry adiabatically in the observational diagnostics. The observational $\langle P_E, K_E \rangle$ are probably under-

estimated due to the underestimated vertical velocities. Since the moist convection was included in the model, the value of $\langle P_E, K_E \rangle$ might be more realistic in the model computation than in the "observational" diagnostics.

The term $\langle K_E, K_Z \rangle$ indicates a transformation from eddy to zonal kinetic energy in the model, in good agreement with the observations. However, the transformation $\langle P_Z, P_E \rangle$, from zonal to eddy available potential energy, seems too low in the model, probably as a result of the low horizontal resolution of the model.

The generation of zonal available potential energy, G_Z, shows good agreement between the model and observations. However, for the generation of eddy available potential energy, G_E, there is a disagreement in sign. The eddy available potential energy is generated by diabatic heating in the model, but is destroyed in the observational diagnostics. Both G_Z and G_E compiled by Saltzman (1970) are from studies of Wiin-Nielsen and Brown (1960) and Brown (1964), in which the two-parameter baroclinic model was used. The two-parameter baroclinic model might underestimate the vertical velocities, which in turn caused an underestimation of the creation of P_E by condensation heating. This is probably the reason why the values of G_E in Saltzman's study appear to be too large and are negative in sign. Furthermore, the values of G_Z and G_E were determined as residuals by Krueger et al.(1965). Thus, these observational values cannot be considered as

reliable standards against which to judge the model.

The kinetic energy dissipations, D_z and D_E, in the model are not in good agreement with those of Saltzman (1970). The total dissipation, $(D_z + D_E)$, is 6.43 watt m^{-2} in the model compared with Saltzman's residual estimate of 3.03 watt m^{-2}. However, based on five-year's data, Kung (1967) suggested a value of 4.94 watt m^{-2} for the winter (October - March) total dissipation, which is in better agreement with the model. But, as the zonal winds in the middle latitudes are much higher in the model than in the observations (Gates, 1972), it is likely that the zonal dissipation, D_z, is somewhat too high in the model.

6.2. Energetics of the control run in the wave-number domain for the region north of $20^{\circ}N$

Fig. 2 shows the ninety-day mean energy budget in the wave-number domain for the winter control run averaged over the area north of $20^{\circ}N$. Except for eddy generation terms, G(n), the model energy flow diagram in the wave-number doamin is qualitatively in good agreement with the observational results of Saltzman (1970). Note that Fig. 2 includes energy flux convergence and pressure interaction terms, which were neglected in the observational results of Saltzman (1970). The general picture is described below.

The available potential energy generated by diabatic heating takes place mainly in the zonal form (G_Z), and flows to all the eddies primarily through eddy sensible heat trans-

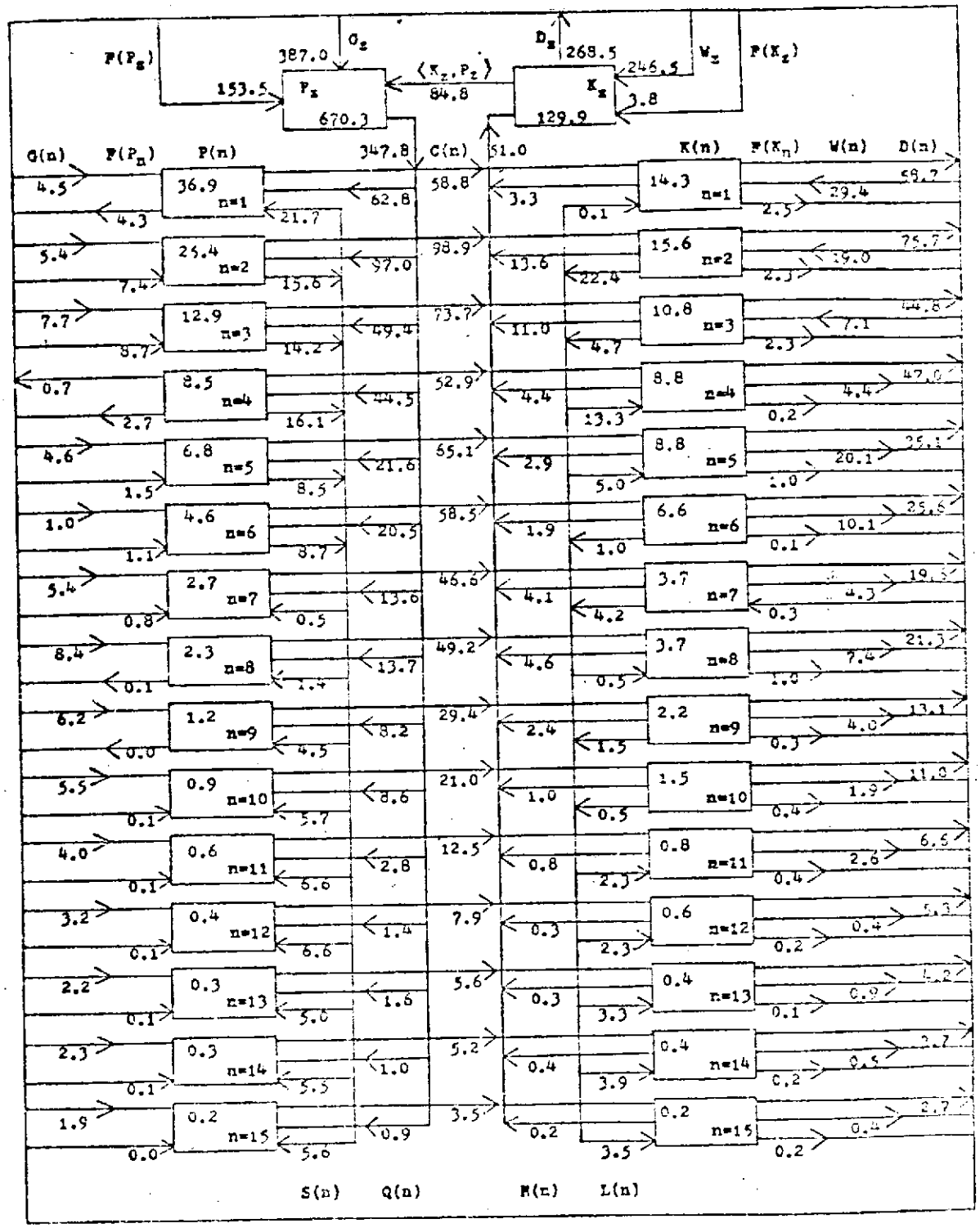

Fig. 2. The ninety-day mean energy budget in the wavenumber domain for the winter control run averaged over area north of 20°N. The unit of energy content is 10^{-4} joules m^{-2} and that of energy transformation is 10^{-2} watts m^{-2}.

fer measured by Q(n), with the dominant transfer in the larger eddies (small wave numbers). The available potential energy is further transferred from longer waves to intermediate and short waves through non-linear wave interactions, S(n). All waves convert their potential energy to kinetic energy through baroclinic processes represented by C(n), and supply kinetic energy to the zonal flow through barotropic processes measured by M(n). Intermediate waves lose kinetic energy, and most longer waves and short waves gain kinetic energy through non-linear wave interactions, L(n).

However, the eddy energies, P(n) and K(n), are generally smaller in the model than in the observations, as are the conversions from P_z to P(n), Q(n). Also, in the non-linear wave interactions, intermediate waves lose less kinetic energy in the model than in the observational diagnostics. Some of these shortcomings of the model are undoubtedly due to the coarse horizontal resolution, as shown by Manabe et al. (1970).

Maximum eddy conversion, C(n), in the model was found in the ultra-long waves (near n=2), whereas the baroclinic instability theory and observational studies (e.g., Saltzman and Fleisher, 1960, 1961) indicate a maximum in the intermediate scale, around n=6. Most of the baroclinic instability theories were based on dry adiabatic models, and the "observational" vertical velocities were computed dry adiabatically. In the study of the effect of sensible heat exchange on the baroclinic instability, Haltiner (1967) found that the heating decreased

the instability at intermediate wavelengths and increased the instability at longer wavelengths. Murakami and Tomatsu (1965) further showed that the most unstable wave could occur at ultra-long waves if sensible heat exchange was taken into consideration. The maximum conversion in the model of Manabe et al. (1970) also takes place in the ultra-long wave, as in the model. The fact that the eddy conversions of the model at all wave numbers are larger than those compiled by Saltzman (1970) is probably also due to the use of dry adiabatic vertical motion in the observational diagnostics.

In summary the model control run exhibits a reasonable and realistic energy budget both in the spatial and wave-number domains for the region north of 20°N.

6.3 Latitudinal distributions of the model energetics

There are more similarities than differences between the energetics of the model control run and those of the model anomaly run. The essential features of the model energetics are reflected in the similarities. Figs. 3-6 show the thirty-day mean latitudinal distributions of energy contents for the control and anomaly runs for the second and third months. Although not shown in figures, the characteristics of the model energetics in the first month is similar to that in the second and third months. There are two maxima of zonal kinetic energy, K_z, in the middle latitudes of both hemispheres reflecting the jet streams in the respective latitudes (Figs. 3A,5A). The eddy kinetic energy, K_E, also has maximum

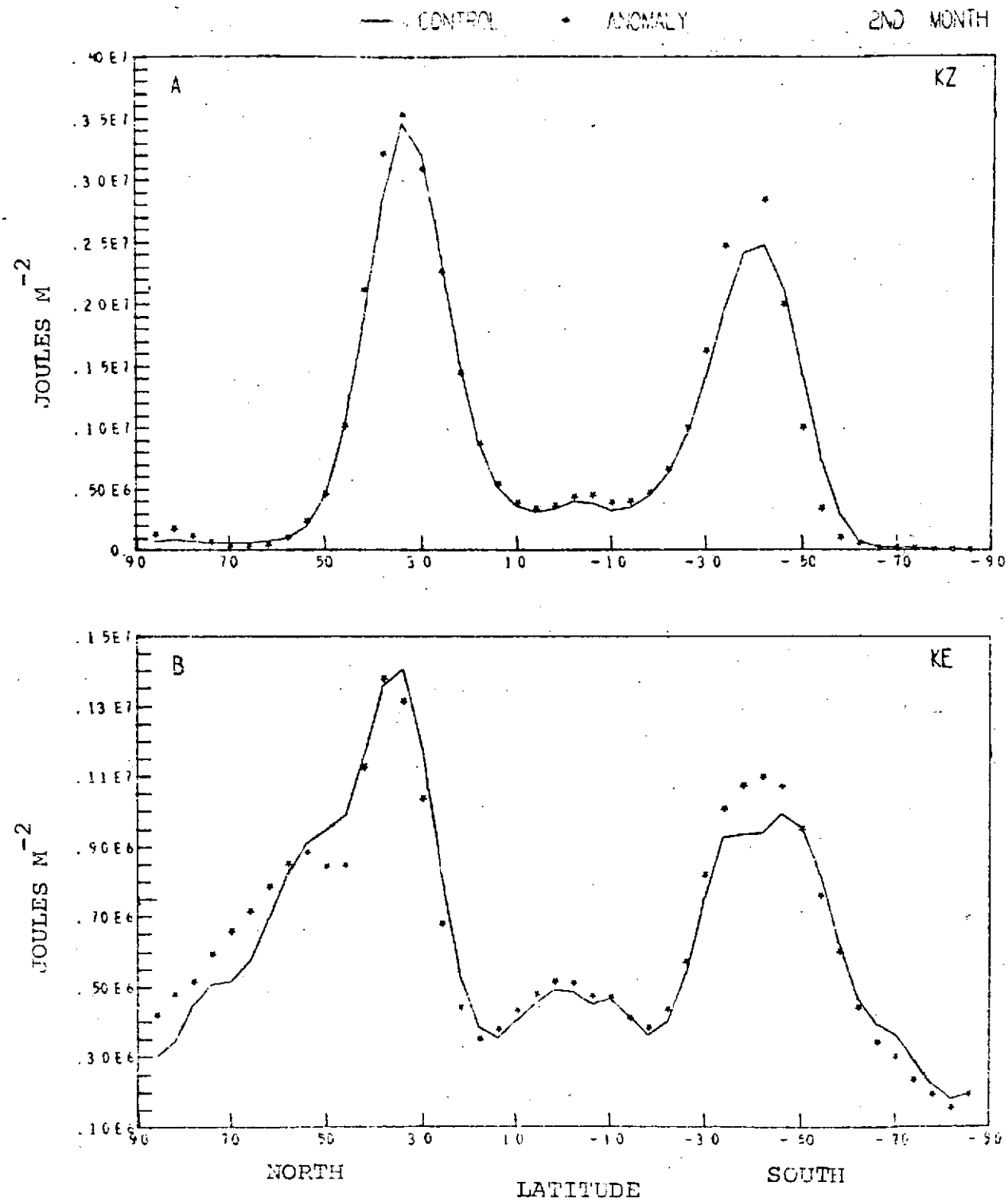

Fig. 3. Thirty-day mean latitudinal distributions of K_Z and K_E for the control and anomaly runs for the second month. (A) Zonal kinetic energy, K_Z. (B) Eddy kinetic energy, K_E.

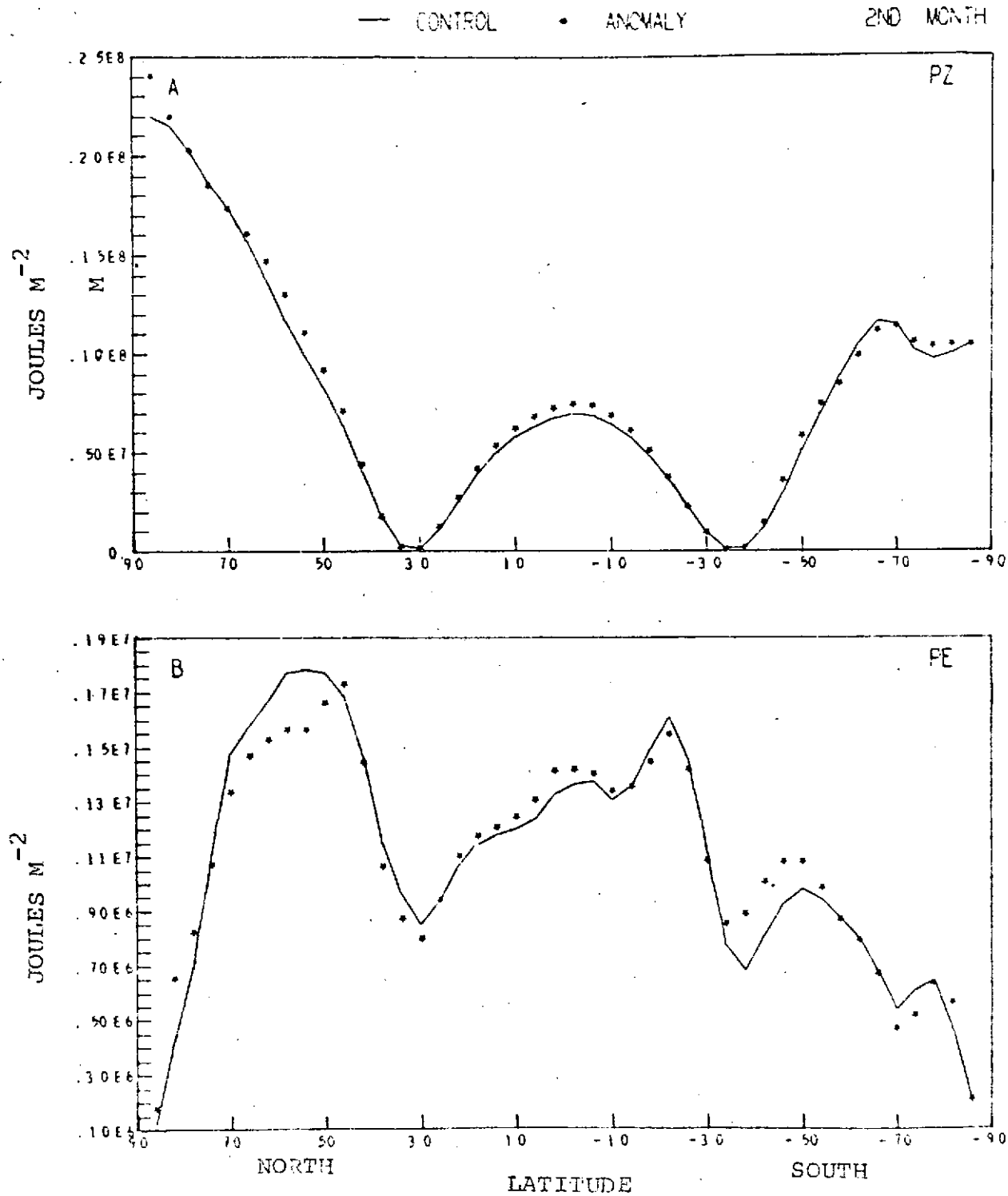

Fig. 4. Thirty-day mean latitudinal distributions of P_Z and P_E for the control and anomaly runs for the second month. (A) Zonal available potential energy, P_Z. (B) Eddy available potential energy, P_E.

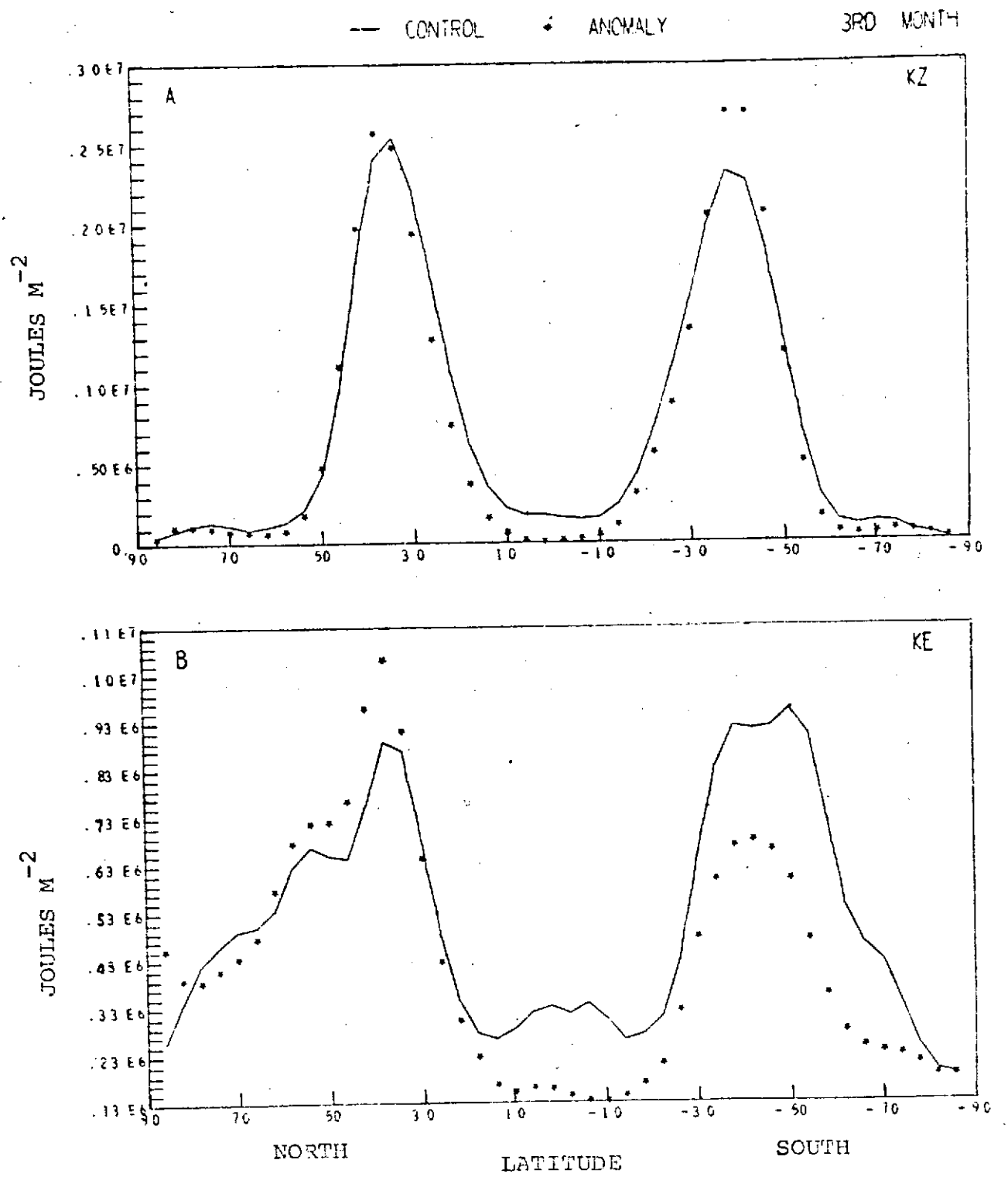

Fig. 5. Same as Fig. 3, for the third month.

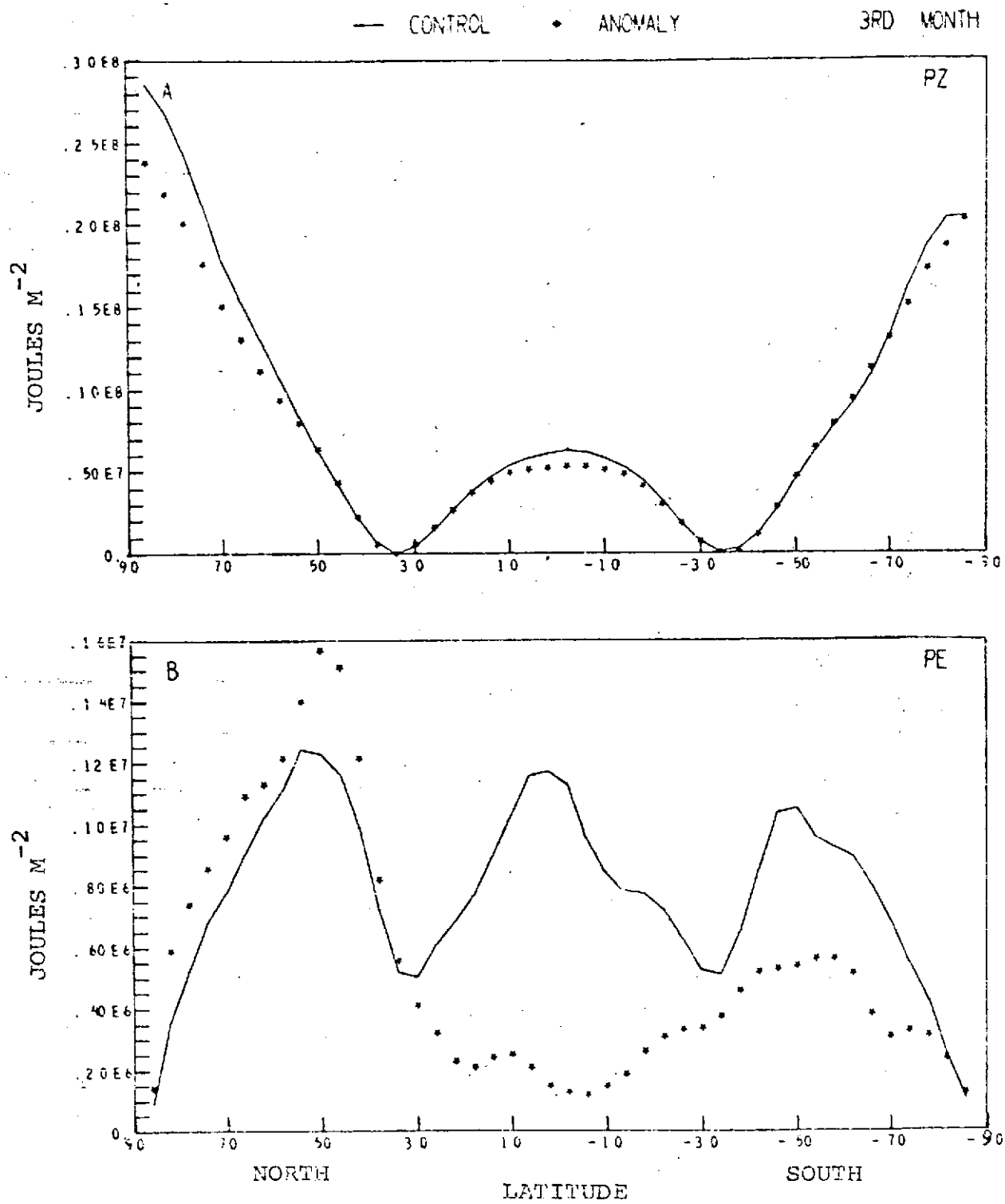

Fig. 6. Same as Fig. 4, for the third month.

values in the northern and southern middle latitudes corresponding to the activities of the extratropical disturbances (Figs. 3B,5B). A minor peak of K_E appears near the equator which shows the activities of tropical disturbances.

The zonal available potential energy, P_Z, has two minima in the middle latitudes of both hemispheres, which are probably too close to the equator due to the excessively high tropical temperatures (Figs. 4A,6A). These two minima could be shifted further pole-wards by improving the convective adjustment to lower the tropical temperatures. In the northern hemisphere winter, the coldest temperature occurs at the north pole, hence, the highest P_Z is found there. The eddy available potential energy, P_E, has maximum values in the middle latitudes of both hemispheres, reflecting the large longitudinal temperature variations in the middle latitudes (Figs. 4B,6B). However, the peak of P_E near the equator is probably exaggerated and is overgenerated by the convective condensation.

Except in the model tropics, the patterns of energies in the model atmospheres are qualitatively in agreement with the observations (e.g., Vincent, 1969).

Figs. 7-16 show the thirty-day mean latitudinal distributions of energy transformations for the second and third months. One noticeable feature is that there exists a spike within the tropical region for most of the energy transformations. There is good reason to believe that these

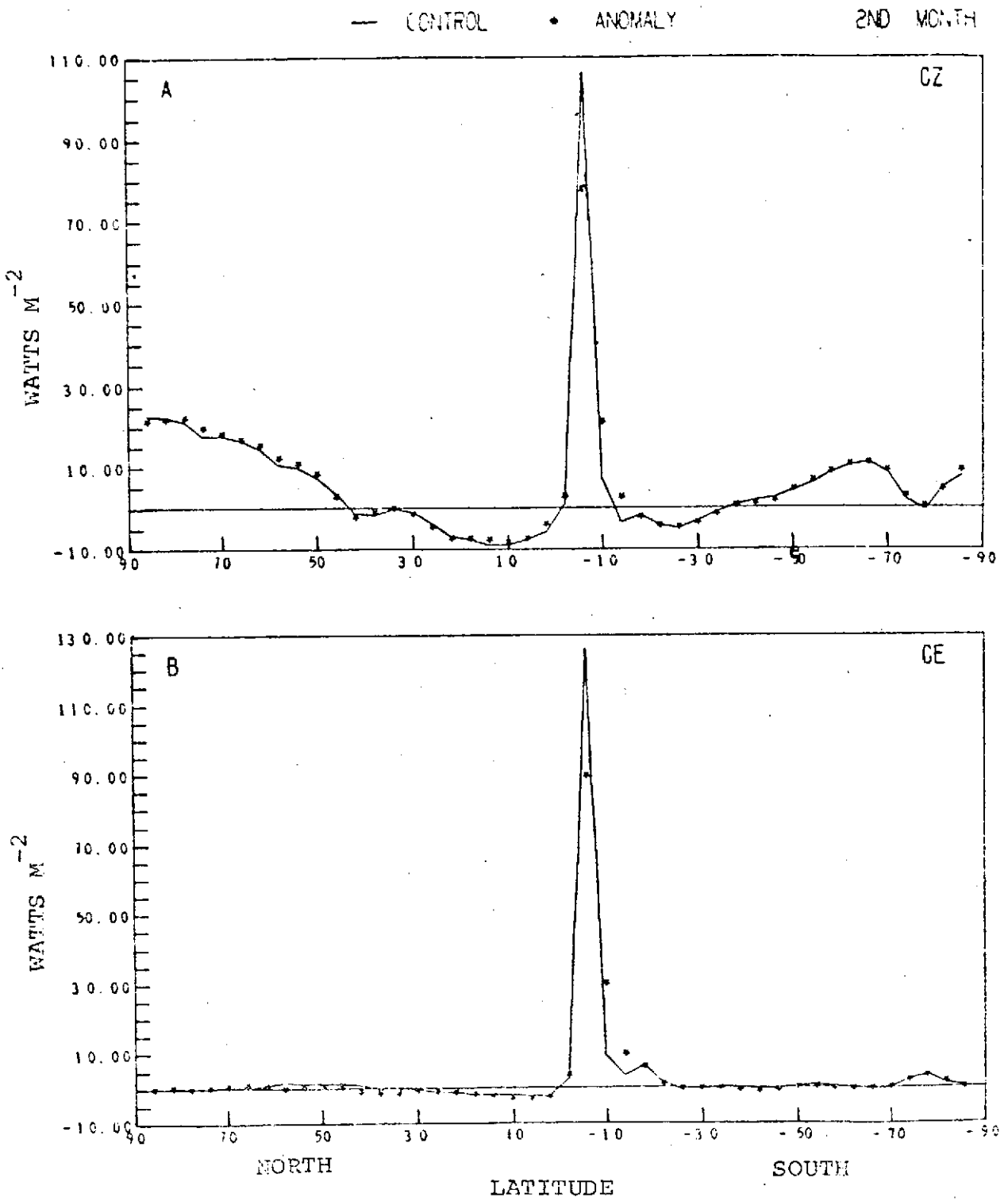

Fig. 7. Thirty-day mean latitudinal distributions of G_Z and G_E for the control and anomaly runs for the second month. (A) Generation of zonal available potential energy, G_Z. (B) Generation of eddy available potential energy, G_E.

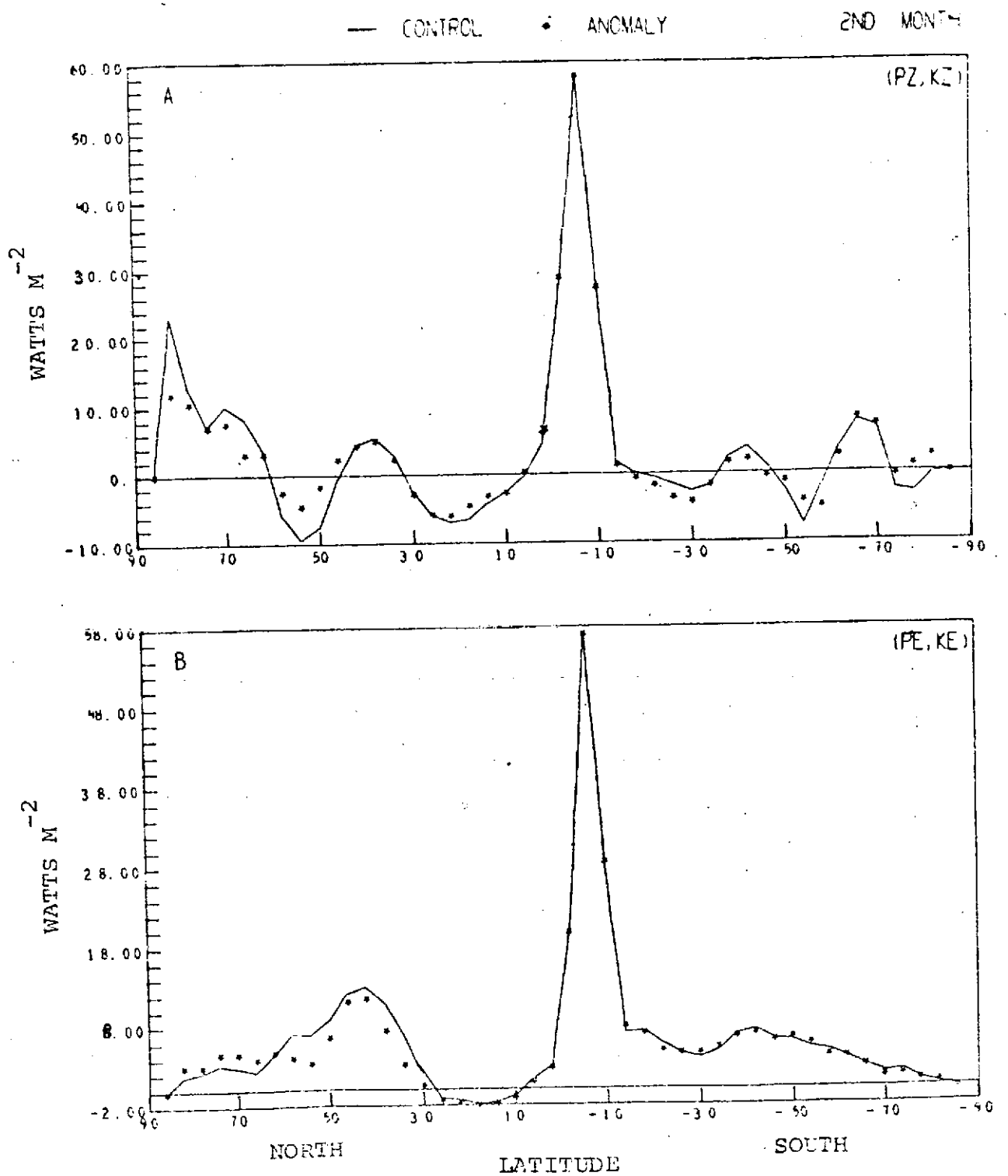

Fig. 8. Thirty-day mean latitudinal distributions of $\langle P_Z, K_Z \rangle$ and $\langle P_E, K_E \rangle$ for the control and anomaly runs for the second month. (A) Conversion from zonal available potential to zonal kinetic energy, $\langle P_Z, K_Z \rangle$. (B) Conversion from eddy available potential to eddy kinetic energy, $\langle P_E, K_E \rangle$.

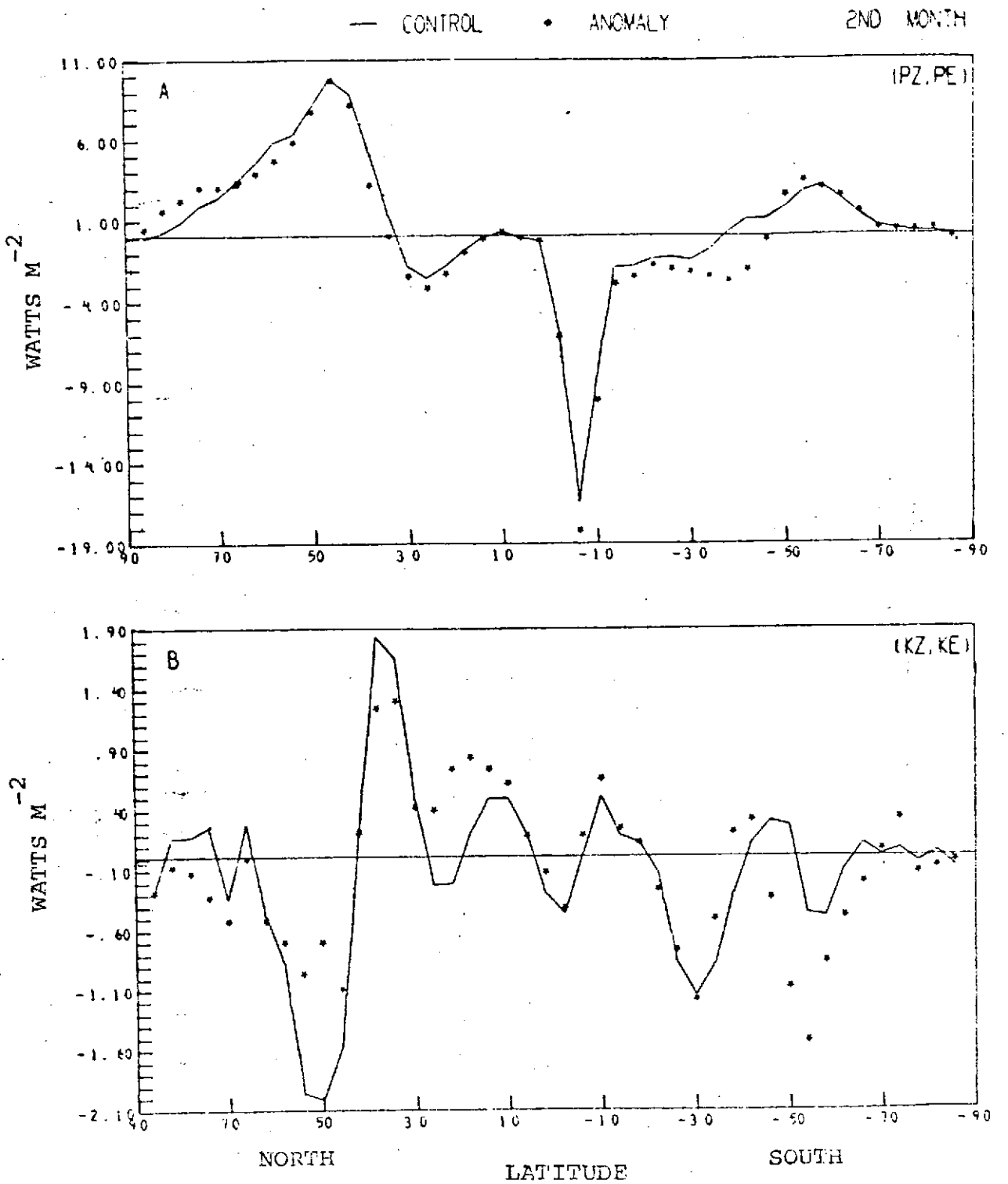

Fig. 9. Thirty-day mean latitudinal distributions of $\langle P_Z, P_E \rangle$ and $\langle K_Z, K_E \rangle$ for the control and anomaly runs for the second month. (A) Conversion from zonal to eddy available potential energy, $\langle P_Z, P_E \rangle$. (B) Conversion from zonal to eddy kinetic energy, $\langle K_Z, K_E \rangle$.

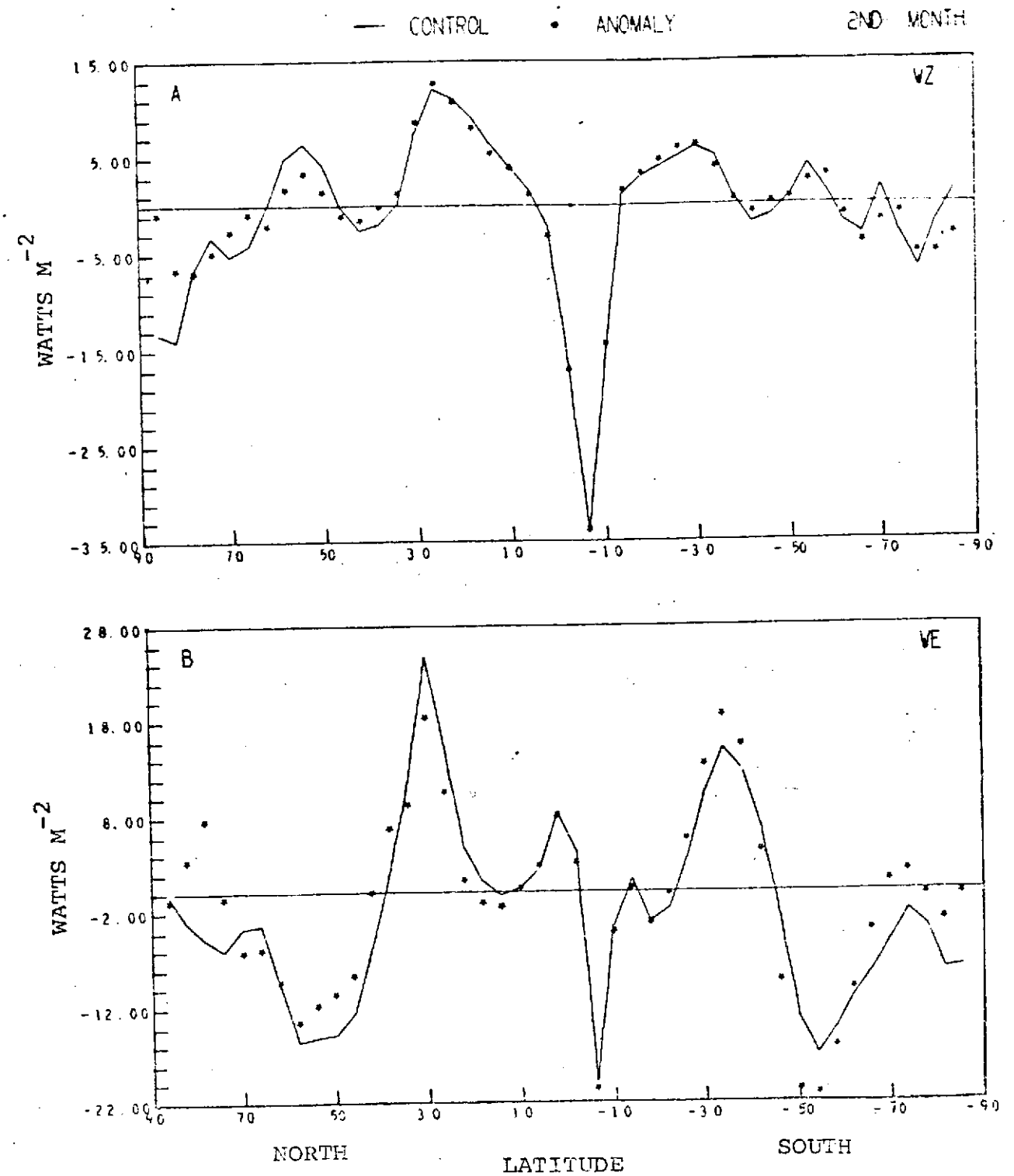

Fig. 10. Thirty-day mean latitudinal distributions of W_Z and W_E for the control and anomaly runs for the second month. (A) Zonal pressure interactions, W_Z. (B) Eddy pressure interactions, W_E.

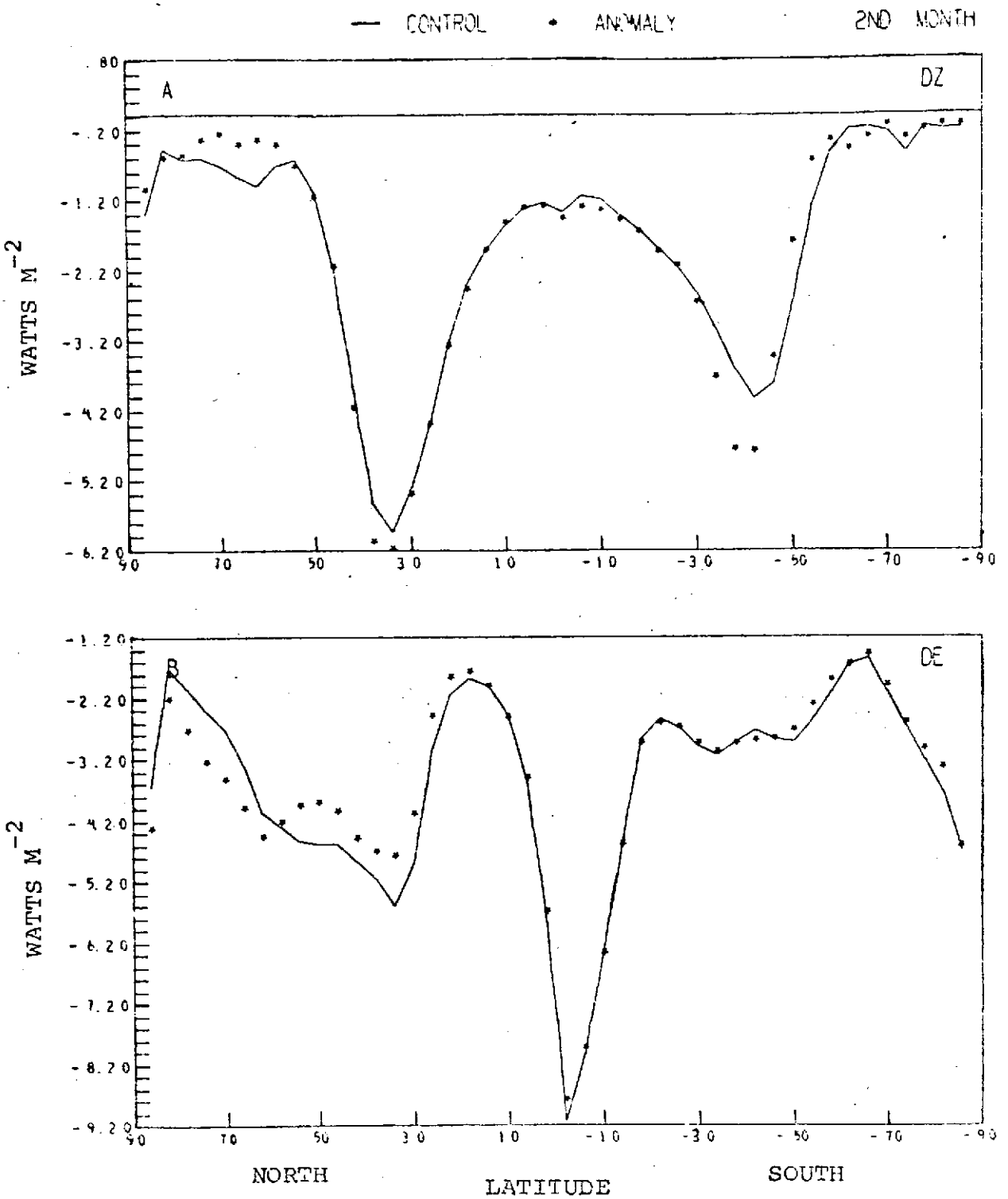

Fig. 11. Thirty-day mean latitudinal distributions of D_Z and D_E for the control and anomaly runs for the second month. (A) Dissipation of zonal kinetic energy, D_Z. (B) Dissipation of eddy kinetic energy, D_E.

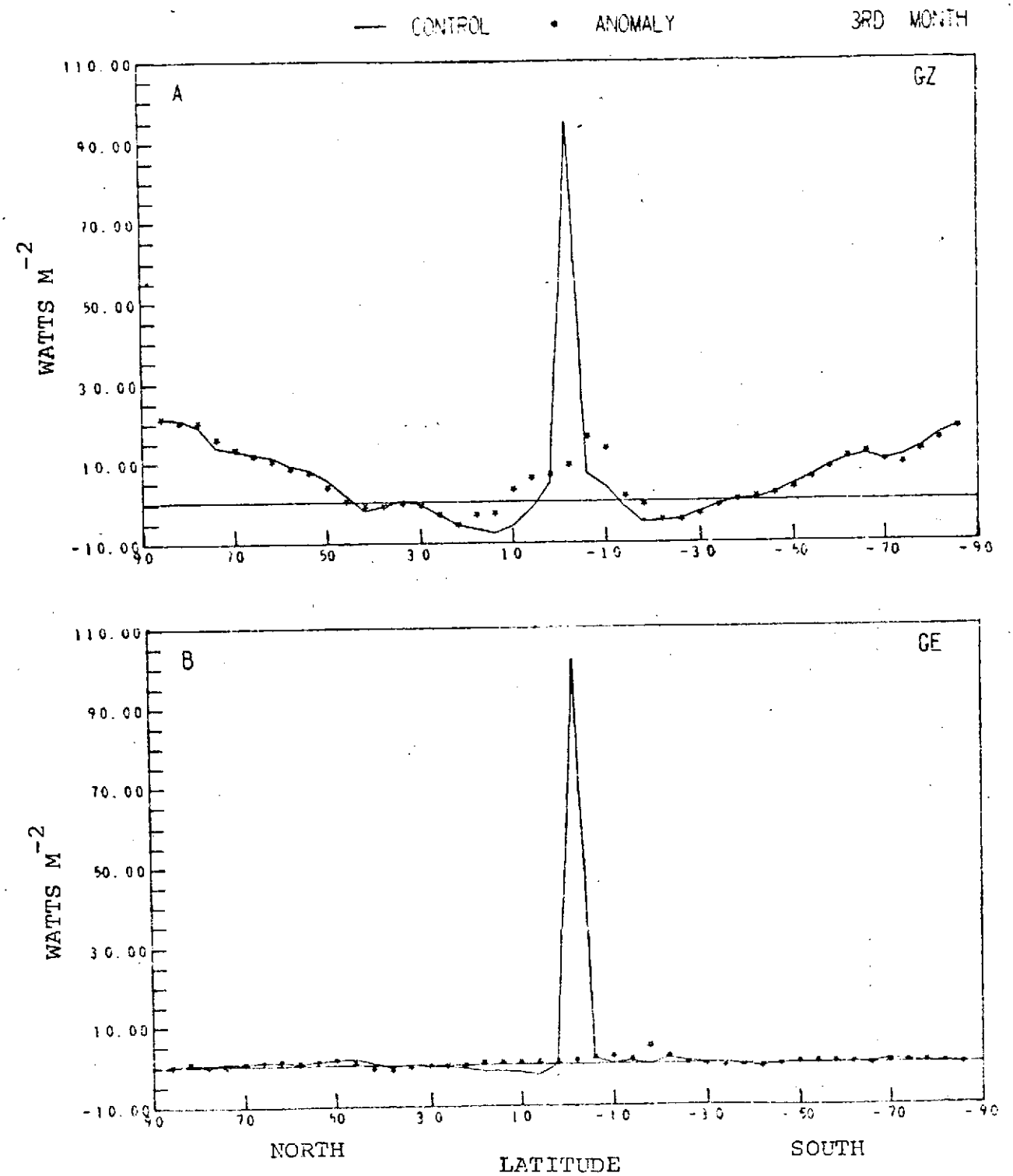

Fig. 12. Same as Fig. 7, for the third month.

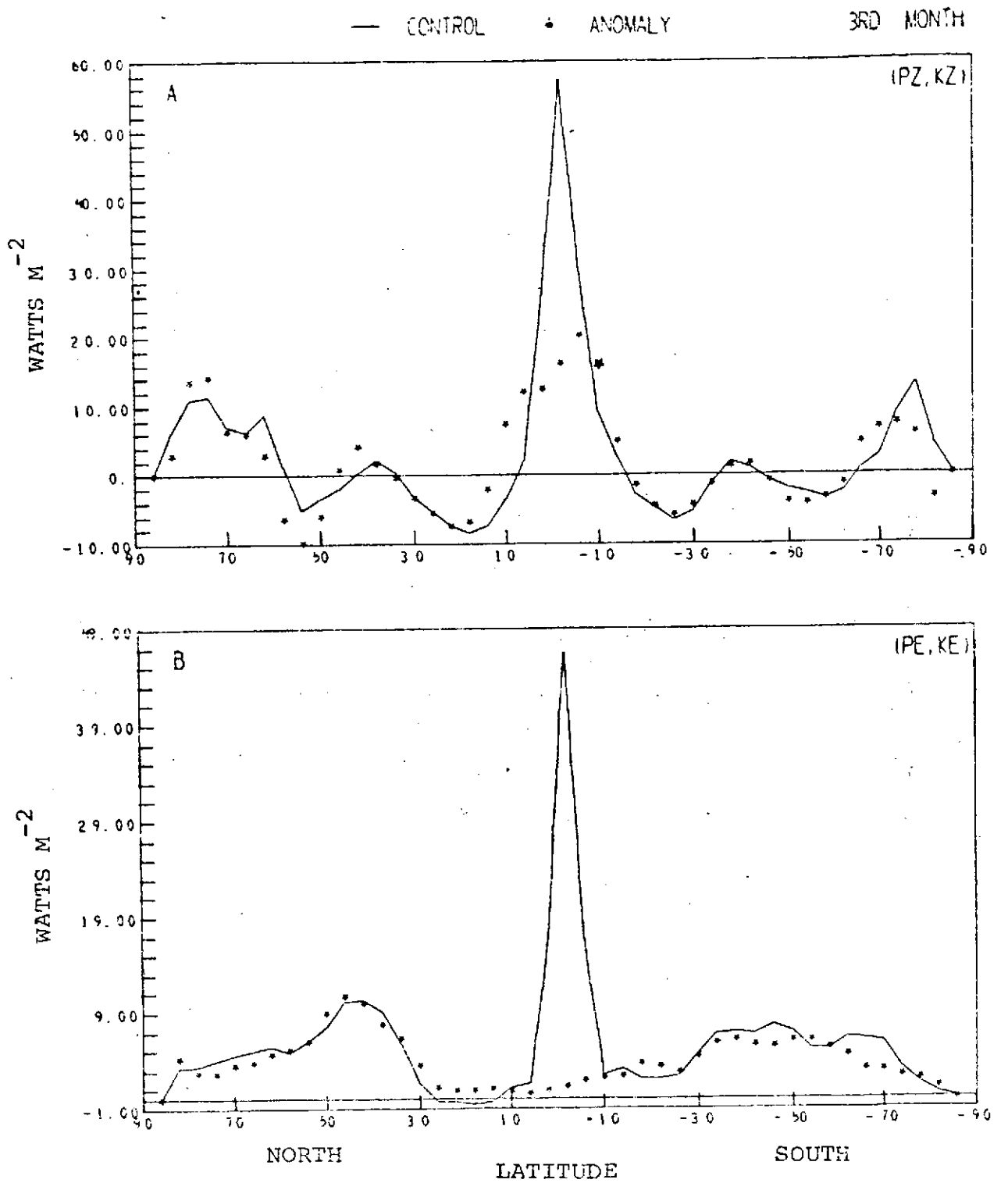

Fig. 13. Same as Fig. 8, for the third month.

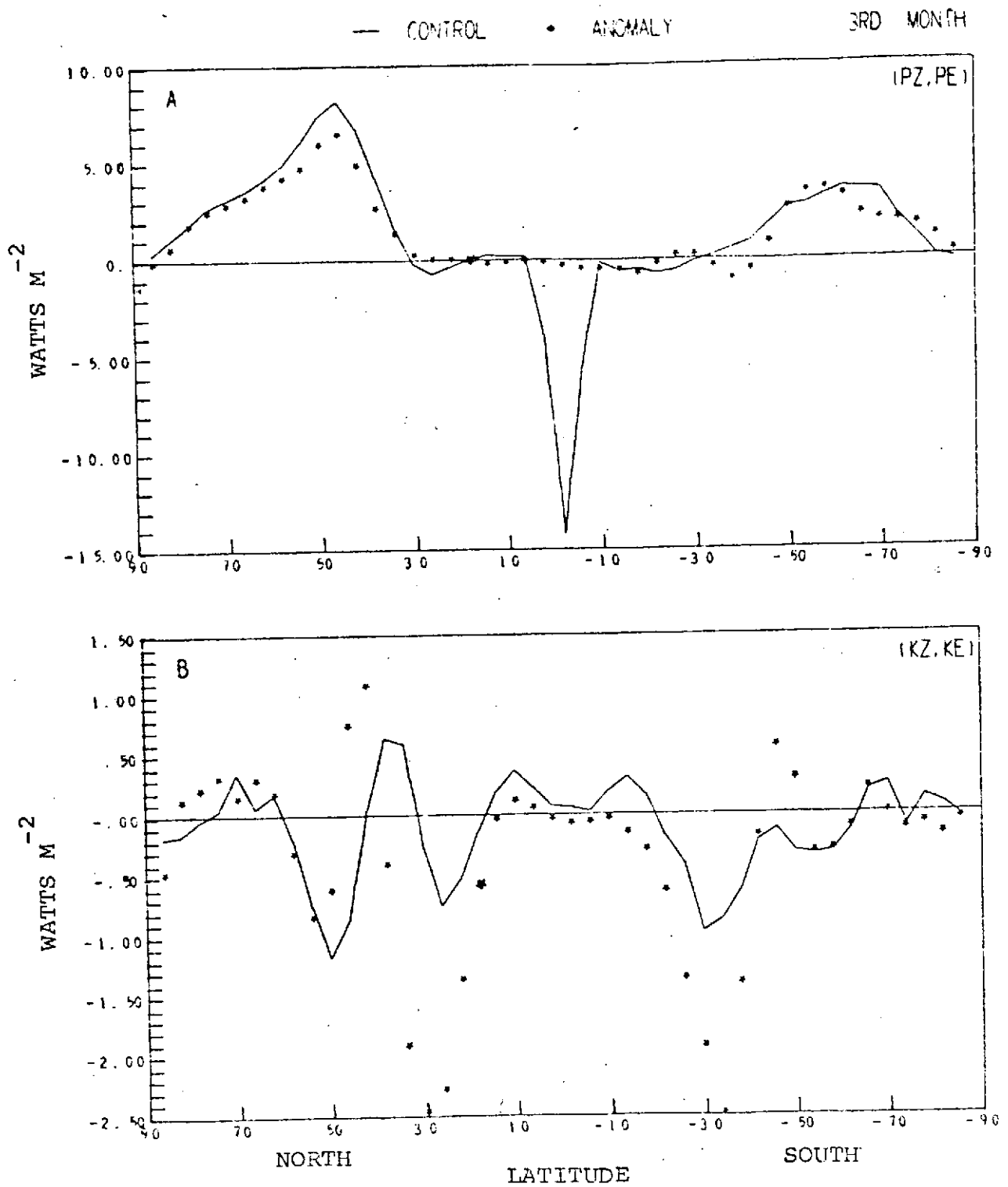

Fig. 14. Same as Fig. 9, for the third month.

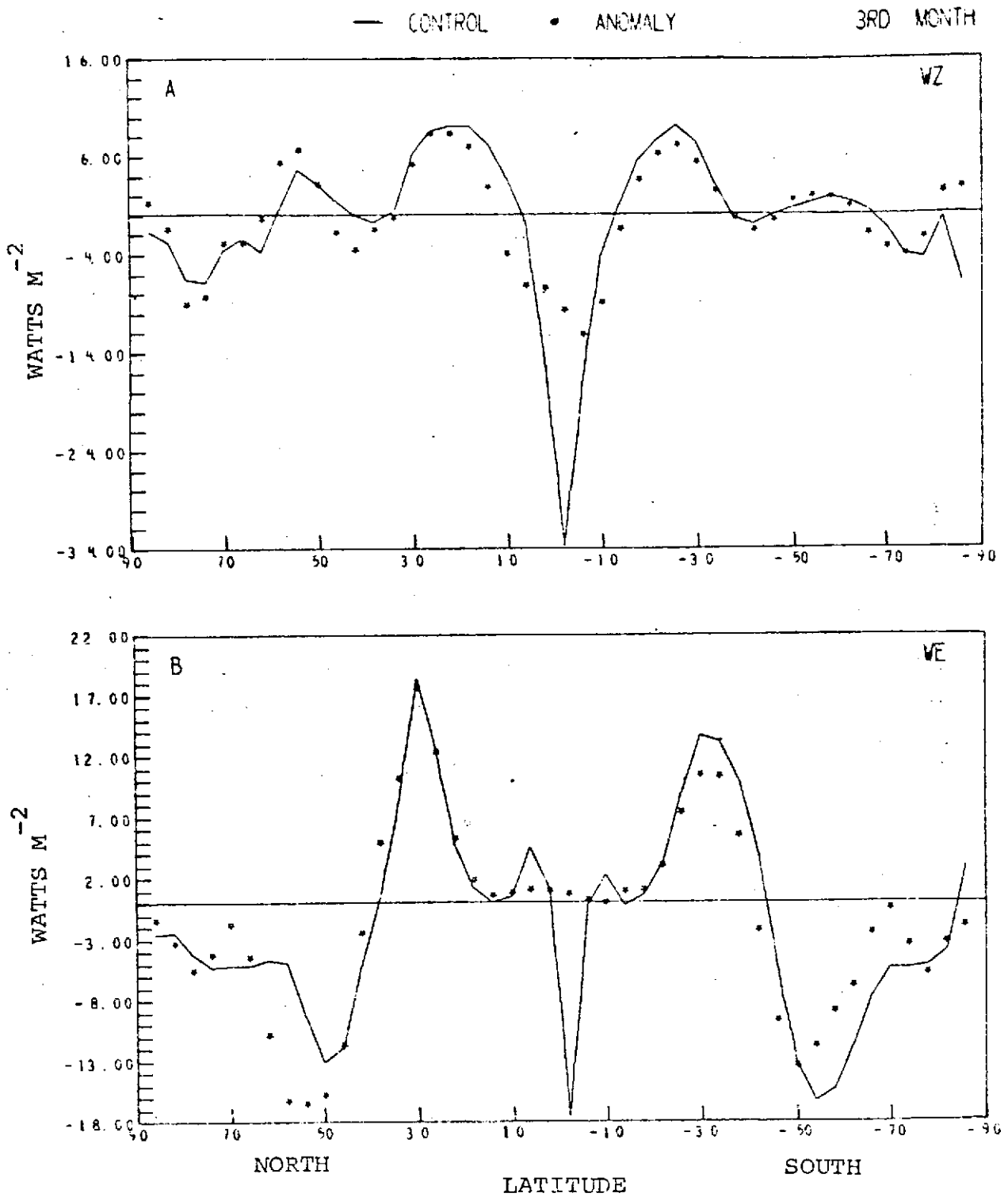

Fig. 15. Same as Fig. 10, for the third month.

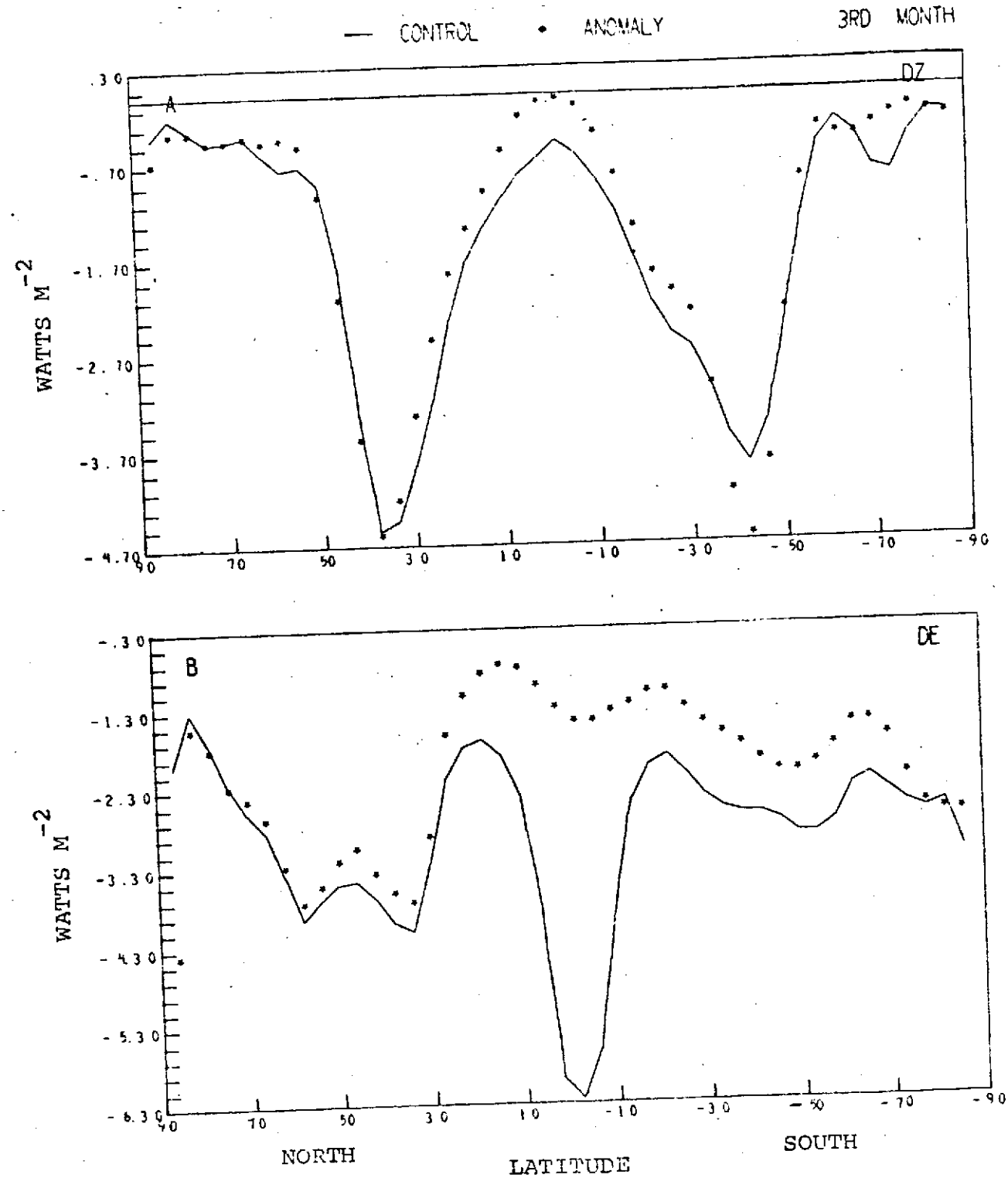

Fig. 16. Same as Fig. 11, for the third month.

reflect a defect in the model, namely the parameterization of convection. The excessive convective condensation in the tropics could overgenerate the available potential energy, and could increase the vertical velocities which in turn intensify the conversion from potential to kinetic energy. These results might further affect other atmospheric processes in the tropics.

In low latitudes the transformation $\langle P_Z, P_E \rangle$ is from eddy to zonal available potential energy, and agrees qualitatively with that proposed by Starr and Wallace (1964). However, its magnitude is probably too large in the model tropics (Figs. 9A, 14A). The eddy dissipation, D_E, in the model tropics is also probably too large for balancing with the exggerated eddy conversion $\langle P_E, K_E \rangle$ (Figs. 8B, 11B, 13B, 16B). The eddy pressure interaction, W_E, in the model tropics even reverse in sign with respect to the results in the general circulation model of Manabe et al. (1970a).

It is generally agreed that zonal available potential energy is generated by low-latitude heating and high-latitude cooling (e.g., Vincent, 1969). However, the model shows that in low latitudes outside the tropical spike, P_Z is destroyed by diabatic cooling (Figs. 7A, 12A). Further investigation shows that in low latitudes the major heating component destroying P_Z is long-wave radiation, which might be too large resulting from the excessively high tropical temperatures. In the middle and high latitudes, the patterns

of G_Z in the model are qualitatively in agreement with the observational results of Vincent (1969) (Figs. 7A, 12A). In high latitudes P_Z is primarily generated by the cooling of long-wave radiation. On the other hand, the patterns of G_E (Figs. 7B, 12B), in the model are determined mainly by condensation processes. Except in the model tropics, the values of G_E are generally small compared with G_Z.

The patterns of $\langle P_Z, K_Z \rangle$ exhibit three-cell meridional circulations in both hemispheres (Figs. 8A, 13A). However, the strength of the Hadley circulations is too strong resulting from the overproduction of convective precipitation in the tropics.

The eddy conversion, $\langle P_E, K_E \rangle$, has maximum values in the middle latitudes of both hemispheres reflecting the extreme baroclinic instability in these regions (Figs. 8B, 13B). The difference of land-sea distributions in both hemispheres and the winter conditions in the Northern Hemisphere enhance the eddy activities in the northern middle latitudes. Thus, the peak values of $\langle P_E, K_E \rangle$ in the northern middle latitudes are larger than those in the southern middle latitudes.

The available potential energy is found to transfer from zonal to eddy in the middle and high latitudes, with the maxima in the middle latitudes (Figs. 9A, 14A). This is qualitatively in agreement with the observational studies (e.g., Oort, 1964; Vincent, 1969; Saltzman, 1970).

The eddy pressure interaction, W_E , acts as a source of eddy kinetic energy in the subtropics and as a sink in the middle and high latitudes (Figs. 10B, 15B). The results in the northern subtropical and middle latitudes are qualitatively in agreement with the results of Manabe et al. (1970a). In the general circulation model of Manabe et al. (1970a), W_E also supplies energy to high latitudes, which is contrary to the results in this study.

The zonal dissipation, D_Z , has maximum values in the middle latitudes reflecting the fact that maximum dissipation occurs in the vicinity of the jet stream (Figs. 11A, 16A). The eddy dissipation, D_E , also has maximum values in the middle latitudes, as expected (Figs. 11B, 16B).

Except in the tropics, the Mintz-Arakawa two layer global general circulation model exhibits a reasonable and realistic energy budget. In the tropics the convective precipitation was found to have a dominating influence on the model energetics. Thus, improvements on the parameterization of convection may bring the simulated tropical energetics closer to the reality.

7. Effects of a transient SST anomaly on the energetics

7.1. Effects on the latitudinal distributions of energetics

The analyses of the sea level pressure pattern and 600 mb geopotential field by Spar (1973, a, b, c) showed that in the first month the responses to the SST anomaly are mainly in the Northern Hemisphere. The analysis of the atmospheric energetics in this study also revealed that in the first month the effects are primarily in the northern middle latitudes. Since the responses are smaller in the first month than in the second and third months, they will be discussed later only in terms of regional analysis. Effects on the latitudinal distributions of energetics for the second and third months are discussed below.

(A) Effects in the second month

In the SST anomaly experiment, a positive SST anomaly was introduced to the anomaly run on the first day of the first month, and was removed from the anomaly run on the first day of the second month. In the first month, with the insertion of the SST anomaly, the portion of the atmosphere above the warm pool tends to gain more sensible heat and water vapor from the underlying sea surface; the surface air above the warm pool is heated gradually by the warm sea. In the second month, with the removal of the SST anomaly, this portion of the atmosphere tends to reduce surface sensible heat flux and evaporation. Therefore, the transient SST anomaly has a heating effect in the first month but has

a cooling effect in the second month in this portion of the atmosphere. These effects then propagate into different parts of the atmosphere through the atmospheric circulations. Since the mean motion of the atmosphere are mainly parallel to latitude circles and the cyclone paths are toward northeast, it is likely that in the second month the cooling effect propagates mostly to the other portions of the northern middle latitudes rather than to other latitude bands.

During the second month, as expected, the anomaly was found to decrease the amount of condensation and eddy generation in the northern middle latitudes (Fig. 7B). It also reduces the energy conversions, $\langle K_z, P_z \rangle$ and $\langle P_E, K_E \rangle$, in the northern middle latitudes (Figs 8A, 8B). The former indicates a reduction in the strength of the Ferrel cell, in which the vertical velocities in the upward branch of the cell are decreased. The latter indicates a decrease in the baroclinic instability, which further causes a decrease in K_E (Fig. 3B). The less active eddies dissipate less energy in the northern middle latitudes (Fig. 11B). The conversion $\langle P_z, P_E \rangle$ in the northern middle latitudes also decreases in the anomaly run compared with the control run (Fig. 9A). This together with the reduction in G_E causes a decrease in P_E (Fig. 4B). Compared with the control run, the zonal pressure interaction, W_z, in the anomaly run appears to supply less energy to the northern middle latitudes (Fig. 10A). On the other hand, W_E in the anomaly run removes less energy

from the northern middle latitudes and supplies less energy to the northern subtropics, compared with the control run (Fig. 10B).

In summary, the transient SST anomaly was found to cause a reduction in the atmospheric processes in the northern middle latitudes during the second month. Apparently, this is the response to the second month's cooling rather than to the first month's warming.

In the second month, the anomaly also affects other area outside the northern middle latitudes, especially the southern middle latitudes. For example, the anomaly appears to cause an increase in K_Z , K_E , P_E , and $\langle K_E, K_Z \rangle$, and a decrease in $\langle P_Z, P_E \rangle$ in the southern middle latitudes (Figs. 3A, 3B, 4B, 9A, 9B). However, the response is less pronounced and less systematic in the area outside the northern middle latitudes.

(B) Effects in the third month

As in the second month, the sea surface temperatures in the third month are the same for both the anomaly and control runs. However, the differences of energetics between the anomaly and control runs are still large. Maximum differences were found in the tropics. In the tropics, all the zonal and eddy energies are decreased in the anomaly run, compared with the control run (Figs. 5, 6). Temperatures in the upper troposphere were found to be much lower in the anomaly run, with a maximum reduction in the tropics. This

results in a lower global mean temperature, and hence P_z is markedly decreased in the tropics (also in high latitudes) (Fig. 6A). The anomaly also appears to reduce wind velocities in the tropics. This can be seen from Figs. 5A and 5B that both K_z and K_E in the tropics are reduced in the anomaly run.

The energy transformations in the tropics are severely distorted in the anomaly run compared with the control run (Figs. 12 - 16). Compared with the control run, the generations, conversions and dissipations in the tropics appear to be less active in the anomaly run. The precipitation and latent heat release in the tropics are due primarily to convective processes. Except at $2^{\circ}S$, the precipitation in the third month in the equatorial region ($20^{\circ}N$ - $20^{\circ}S$) appears to be larger in the anomaly run than in the control run. However, at $2^{\circ}S$, where all the energy transformations show dramatic reductions, the decrease of precipitation in the anomaly run was extremely large (about 80%). Since the convective condensation is the major component for generating P_z and P_E in the tropics, the dramatically altered convective condensation markedly changes the patterns of G_z and G_E in the tropics in the anomaly run (Figs. 12A, 12B). These changes further affect all the other energy transformation processes in the tropics. Because of the unsatisfactory parameterization of convection in the model (Gates, 1972), it is very likely that this tropical effect is a computational artifact caused by a model defect rather than a true reflec-

tion of nature.

In the third month the influence of the SST anomaly in the northern middle latitudes is not so pronounced and systematic as in the second month. Nevertheless, some responses can still be found. Both K_E and P_E in the northern middle latitudes appear to be larger in the anomaly run than in the control run (Figs. 5B, 6B). As can be seen from the pattern of $\langle P_Z, K_Z \rangle$, the indirect Ferrel cell in the northern middle latitudes is intensified in the anomaly run (Fig. 13A). Compared with the control run, it was found that W_E in the anomaly run transports more energy out of the northern middle latitudes (Fig. 15B). However, the conversion from P_Z to P_E in the northern middle latitudes is reduced in the anomaly run (Fig. 14A).

For the southern middle latitudes, on the contrary, the response to the SST anomaly is more apparent and more systematic in the third month than in the second month. The transient Northern Pacific warm pool appears to cause a decrease in the eddy activity in the southern middle latitudes during the third month. This is shown in the reductions of K_E, P_E, $\langle P_E, K_E \rangle$, $\langle P_Z, P_E \rangle$, and D_E in the southern middle latitudes in the anomaly run (Figs. 5B, 6B, 13B, 14A, 16B). The pattern of W_E also reveals the reduction of eddy activity in the southern middle latitudes. The eddy pressure interaction in the anomaly run removes less energy out of the southern middle latitudes, and supplies less energy to the

subtropics of the Southern Hemisphere (Fig. 15B). The conversion $\langle K_E, K_Z \rangle$ in low latitudes of about $40^{\circ}S - 40^{\circ}N$ appears to be increased by the transient SST anomaly.

Although the anomalous pattern of the sea surface temperature field persists for a period of only one month, the results for the second and third months suggest that the transient SST anomaly can indeed have a disturbing effect on the global energetics.

7.2. Effects on the regional energetics

It is well known (Mintz et al., 1972) that the two-level Mintz-Arakawa model produces a poor simulation of the climate in the polar and tropical regions. It is also a fact that (except for the dubious tropical response in the third month) the transient North Pacific SST anomaly in the experiment produces a maximum response in the middle latitudes. Because of these two reasons, two zonal sections representing middle latitudes were particularly chosen for detailed analysis. These two zonal sections are $28^{\circ}N - 60^{\circ}N$ and $28^{\circ}S - 60^{\circ}S$. The effects in these two areas are discussed in terms of gross regional energetics both in the spatial and wave-number domains.

(A) Effects in the northern middle latitudes

The thirty-day mean energetics for each month of the control and anomaly runs in the zonal section $28^{\circ}N - 60^{\circ}N$ are shown in Table 3. Figs. 17, 18, and 19 illustrate the thirty-day mean spectral distributions of K(n), P(n), N(n),

Table 3. Thirty-day mean energetics for each month of the control and anomaly runs in the zonal section $28^{\circ}N - 60^{\circ}N$. The unit of energy content is 10^{4} joules m^{-2} and that of energy transformation is 10^{-2} watt m^{-2}.

	Control	Anomaly	Control	Anomaly	Control	Anomaly
Month No.	1	1	2	2	3	3
P_z	418	422	468	517	354	339
P_E	122	131	138	129	89	104
K_z	169	171	183	192	147	149
K_E	100	100	113	106	73	82
G_z	177	152	295	321	230	177
G_E	77	108	89	0	84	38
W_z	78	66	222	185	208	151
W_E	-201	-187	-120	43	-98	-186
$\langle K_z, P_z \rangle$	335	307	100	-64	112	191
$\langle P_E, K_E \rangle$	1014	1058	852	600	690	729
$\langle P_z, P_E \rangle$	555	571	512	425	460	363
$\langle K_E, K_z \rangle$	79	91	11	-8	19	65

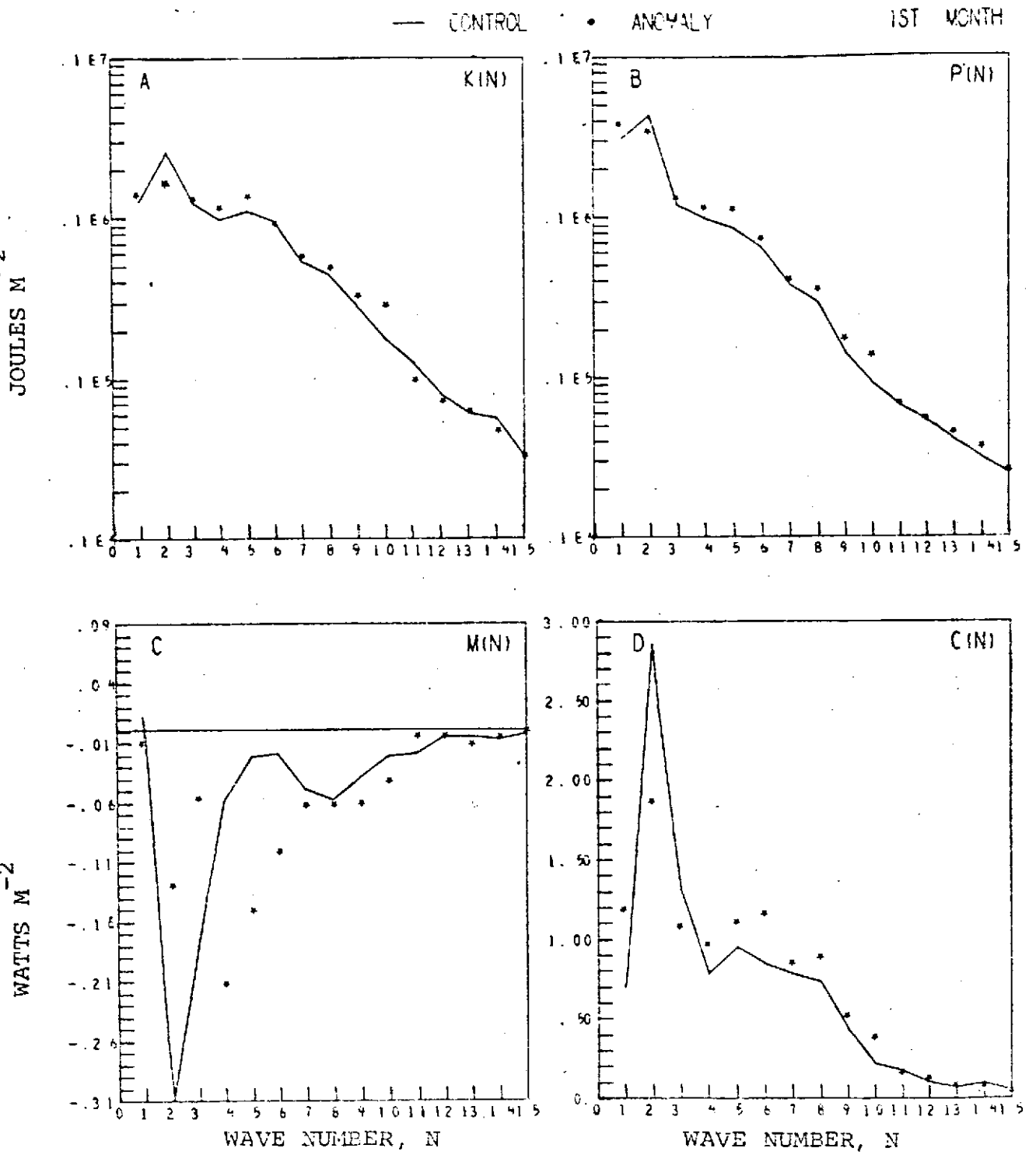

Fig. 17. Thirty-day mean spectral distributions of K(n), P(n), M(n), and C(n) for the control and anomaly runs for the first month in the zonal section 28°N-60°N. (A) Spectral component of eddy kinetic energy, K(n). (B) Spectral component of eddy available potential energy, P(n). (C) Conversion from zonal kinetic energy to K(n), M(n). (D) Conversion from P(n) to K(n), C(n).

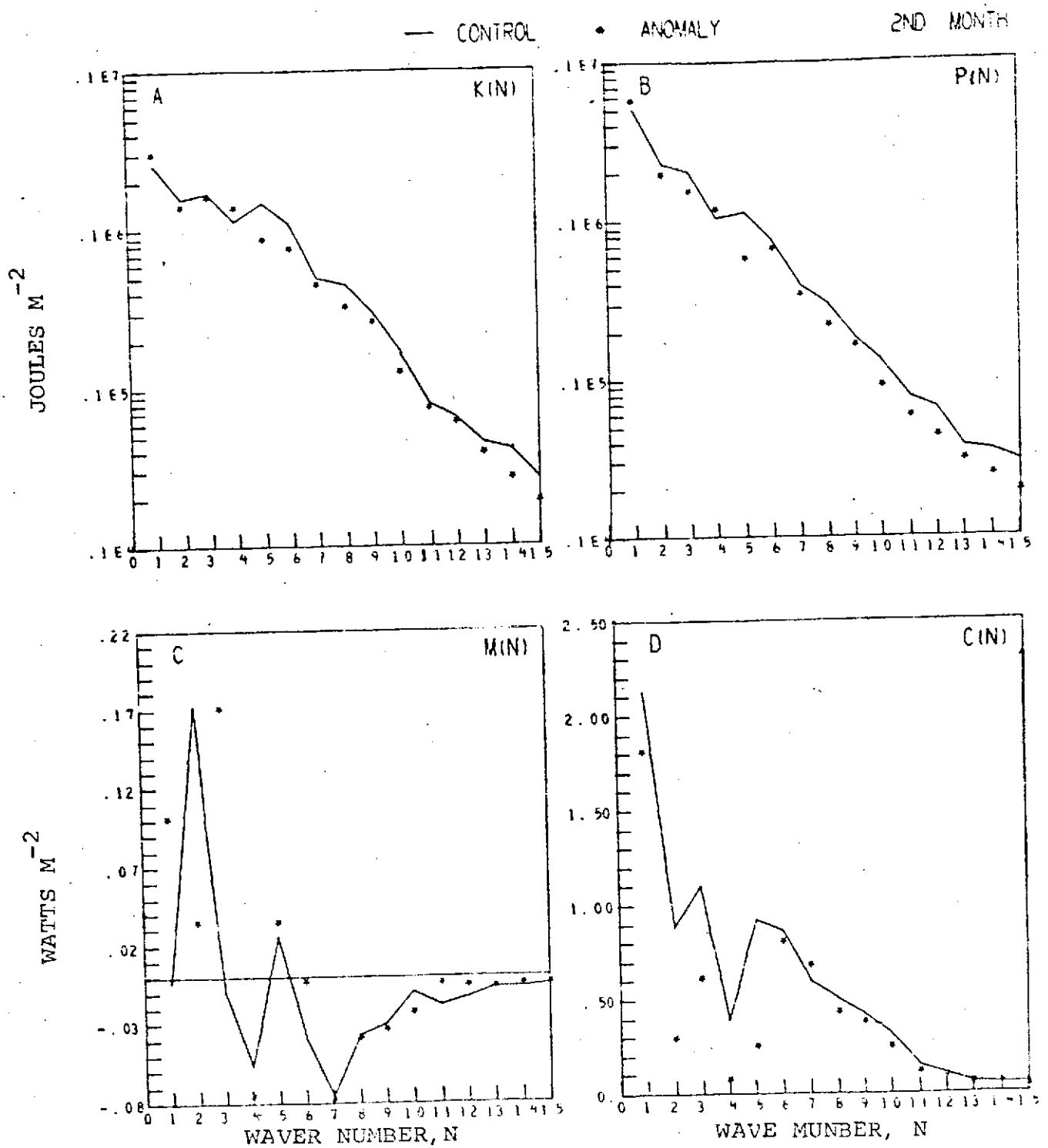

Fig. 18. Same as Fig. 17, for the second month.

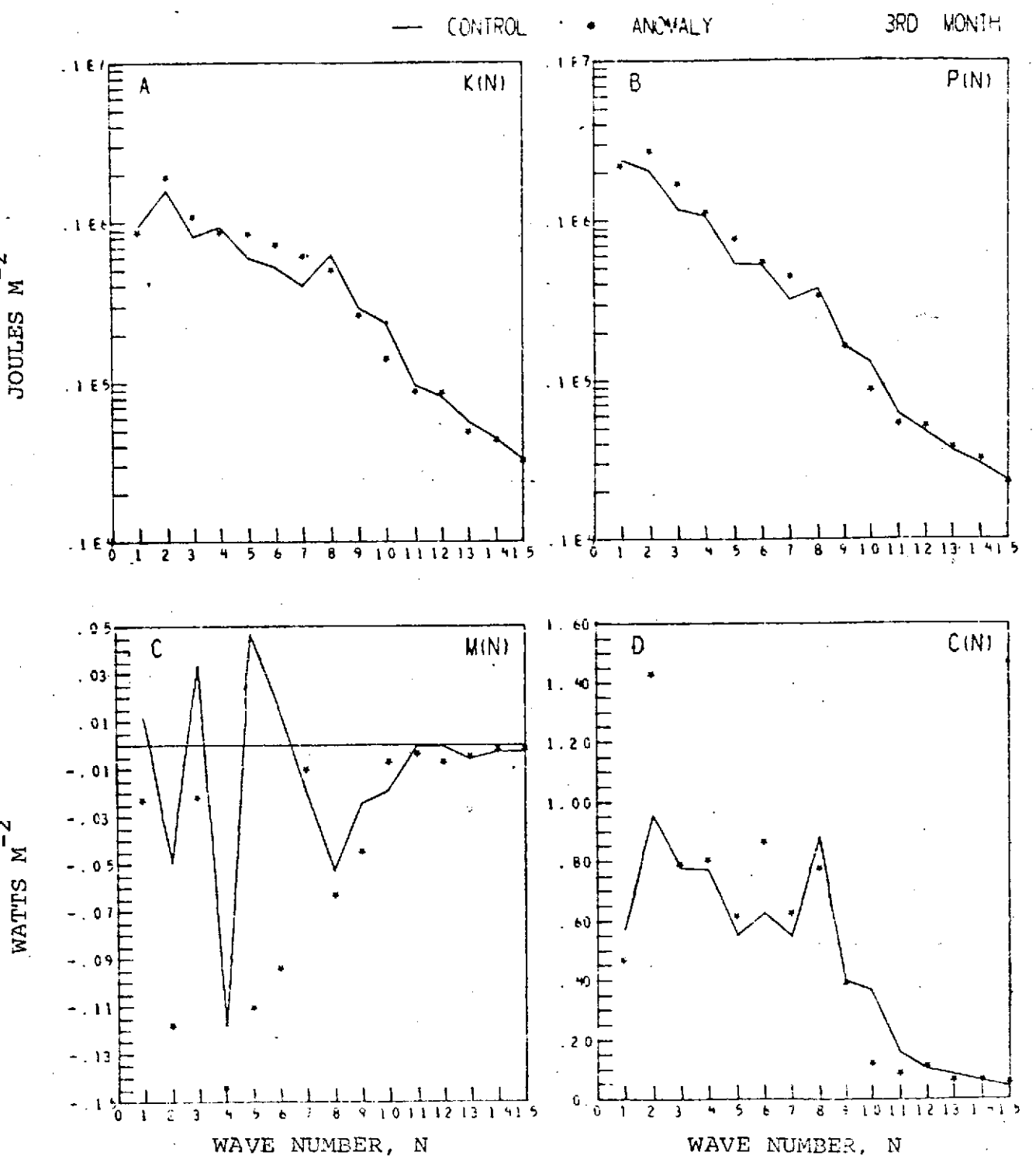

Fig. 19. Same as Fig. 17, for the third month.

and C(n) for each month of the control and anomaly runs in the same zonal section. K(n) and P(n) are the spectral components of K_E and P_E, respectively, and M(n) and C(n) the spectral components of $\langle K_Z, K_E \rangle$ and $\langle P_E, K_E \rangle$, respectively.

Table 3 indicates that in the first month the effects in the northern middle latitudes are fairly small compared with the other two months. In the first month, the transient SST anomaly appears to cause an increase in P_E and G_E, as was expected, and a slight reduction in G_Z, together with slightly increased conversions from P_Z to P_E, P_E to K_E, and K_E to K_Z. However, during the first month the spectral energetics in the northern middle latitudes are greatly disturbed by the SST anomaly (Fig. 17). As might have been expected, the anomaly appears to cause an increase in the eddy activity of the intermediate scales. In the intermediate scales (n=4 - 10), eddy energies, K(n) and P(n), and eddy conversion, C(n), are increased in the anomaly run (Figs. 17A, 17B, 17D). On the northern side of the warm pool, the sea surface temperature gradients are increased in the first month by the prescribed SST anomaly. This increases the baroclinic instability and eddy conversion around the intermediate scales. The more active cyclone waves then transfer more kinetic energy to zonal flow to maintain the zonal wind system (Fig. 17C). Although not shown in the figures, the spectral analysis reveals that the increase of G_E takes place mainly in wave number 1 and 2. This increase is due primarily

to the increased latent heat released by condensation.

Another noticeable feature occuring in the first month is that the eddy activity of the ultra-long waves is markedly reduced in the anomaly run, especially wave number 2 (Fig. 17). Because most of the increase of eddy activity around the intermediate scales is compensated by the reduction in ultra-long waves, the net eddy activity shows only a minor increase in the northern middle latitudes (Table 3). Heat sources and sinks of planetary dimensions are very important for determining large-scale flow patterns (e.g., Smagorinsky, 1953). Large-scale flow patterns are generally dominated by the long planetary waves. The SST anomaly in the first month probably cause a considerable change in the distribution of large-scale heat sources and sinks. This then produces a larger dynamical response in the ultra-long waves. However, the way that ultra-long waves respond to SST anomalies is not so easy to anticipate, unlike the responses of the intermediate cyclone waves, which can be inferred from baroclinic instability theory.

In the second month, as indicated in Table 3, the responses in the northern middle latitudes are more apparent. The anomaly causes eddy generation, G_E , to reduce to zero in the anomaly run. It alsc causes $\langle K_z, P_z \rangle$, $\langle K_E, K_z \rangle$, and W_E to change sign. The change of $\langle K_z, P_z \rangle$ indicates a direct energy conversion replaced the normal indirect energy conversion. The reduction in the strength of the upward

branch of the Ferrel cell is responsible for this change (Fig. 8A). The reversal in sign of $\langle K_E, K_z \rangle$ indicates an anomalous conversion from zonal to eddy kinetic energy. These changes together with a reduction in K_E , P_E , $\langle P_E, K_E \rangle$, and $\langle P_z, P_E \rangle$ clearly indicates that the transient SST anomaly has a effect of reducing eddy activity in the northern middle latitudes after a period of one month. The spectral analysis reveals that the reduced eddy activity takes place at all wave numbers, with the major reduction in the longer waves (Fig. 18). From Fig. 18 it can be seen that K(n), P(n), and C(n) (also eddy generation, G(n), but not shown in the figures) decrease over almost all waves, with the dominant reduction in the longer waves. In a barotropic atmosphere, the unstable eddy receives its energy from zonal kinetic energy (e.g., Kuo, 1949; Brown, 1969). Fig. 18C illustrates the fact that the anomaly causes the eddy of wave number 2 to become less barotropically unstable, but causes the eddies of wave number 1 and 3 to become more barotropically unstable. The reversal in sign of $\langle K_E, K_z \rangle$ is due primarily to the changes in wave number 1 and 3.

In the third month, as can be seen from Table 3, G_z , G_E , and $\langle P_z, P_E \rangle$ in the northern middle latitudes are reduced in the anomaly run, but P_E , K_E , and $\langle K_E, K_z \rangle$ are increased by the transient Northern Pacific warm pool. The anomaly also intensifies the indirect Ferrel cell and causes eddy pressure interaction to transport more energy out of

northern middle latitudes. During the third month, the eddy activity is generally increased in the northern middle latitudes. In the wave-number domain, this increase takes place from n=2 to n=7 (Fig. 19). Fig. 19 illustrates an increase of K(n), P(n), and C(n), and a decrease of N(n) at these waves. Among those waves, eddy conversions at wave number 2 and 6 are particularly increased in the anomaly run (Fig. 19D). Also, all the waves were found to transfer kinetic energy to zonal flow in the anomaly run, while zonal flow supplies energy to eddies of wave number 1, 3, 5 and 6 in the control run (Fig. 19C). This is why $\langle K_E, K_Z \rangle$ is increased in the anomaly run.

(B) Effects in the southern middle latitudes

The thirty-day mean energetics for each month of the control and anomaly runs in the zonal section 28°S - 60°S are shown in Table 4. The thirty-day mean spectral distributions of K(n), P(n), N(n), and C(n) for each month of the control and anomaly runs in the same region are illustrated in Figs. 20, 21, and 22. The gross regional energetics both in the spatial and wave-number domains show that the effects in the southern middle latitudes are very small during the first month (Table 4, Fig. 20).

In the second month, the most noteworthy effects of the transient SST anomaly in the southern middle latitudes are the reversal in sign of $\langle P_Z, P_E \rangle$, and the large decrease in W_E (Table 4). The anomaly also increases the conversions

Table 4. Thirty-day mean energetics for each month of the control and anomaly runs in the zonal section $28^{\circ}S - 60^{\circ}S$. The unit of energy content is 10^{4} joules m^{-2} and that of energy transformation is 10^{-2} watt m^{-2}.

	Control	Anomaly	Control	Anomaly	Control	Anomaly
Month No.	1	1	2	2	3	3
P_Z	209	226	286	305	250	259
P_E	84	80	89	98	78	47
K_Z	153	152	168	180	161	168
K_E	73	72	88	94	85	57
G_Z	119	127	210	199	185	174
G_E	53	46	31	13	35	28
W_Z	141	140	202	219	183	145
W_E	-27	-85	160	34	61	-116
$\langle K_Z, P_Z \rangle$	101	91	95	138	149	163
$\langle P_E, K_E \rangle$	665	644	556	573	628	561
$\langle P_Z, P_E \rangle$	99	108	78	-38	129	87
$\langle K_E, K_Z \rangle$	47	46	36	59	51	82

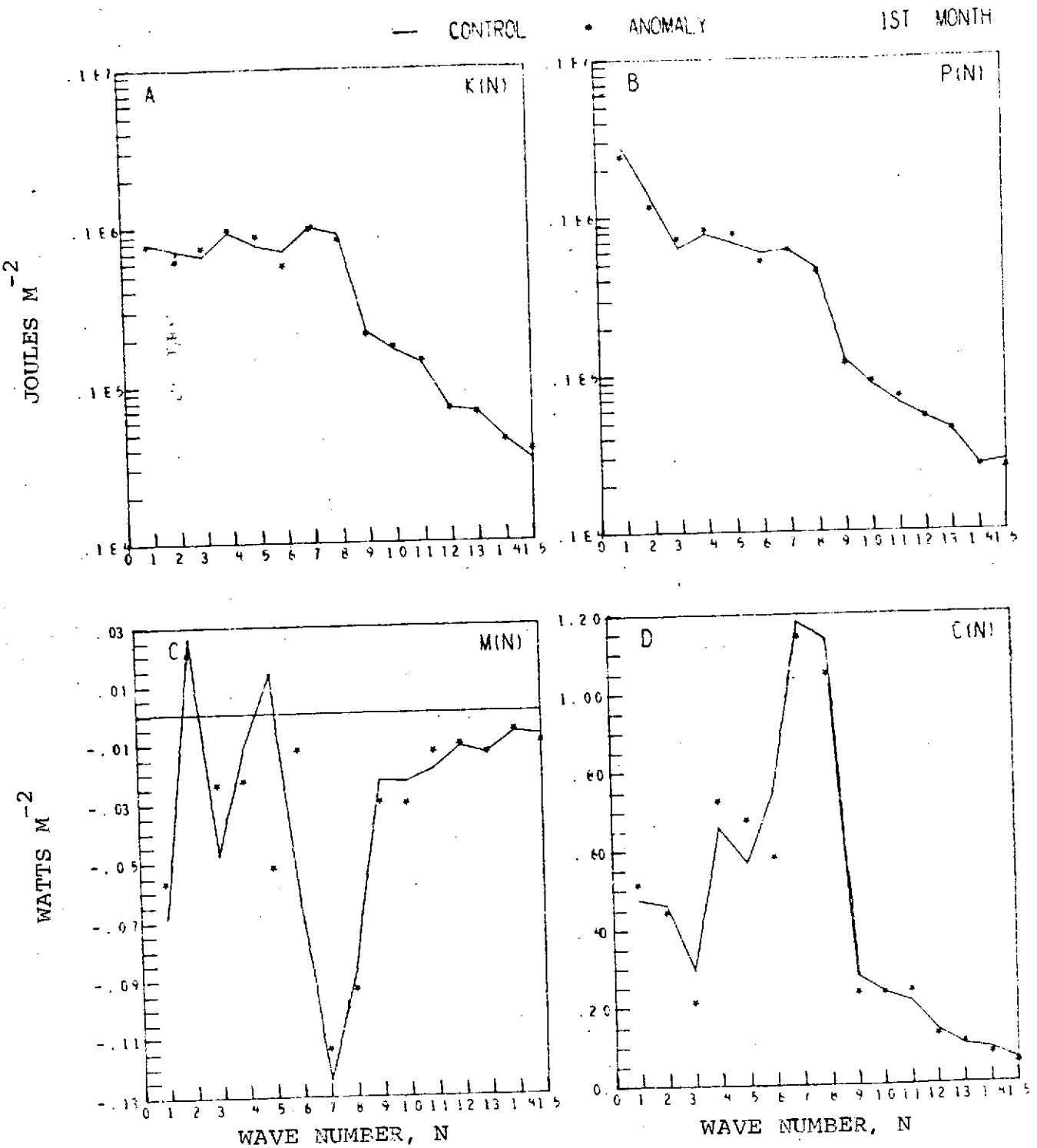

Fig. 20. Same as Fig. 17, in the zonal section 28°S-60°S.

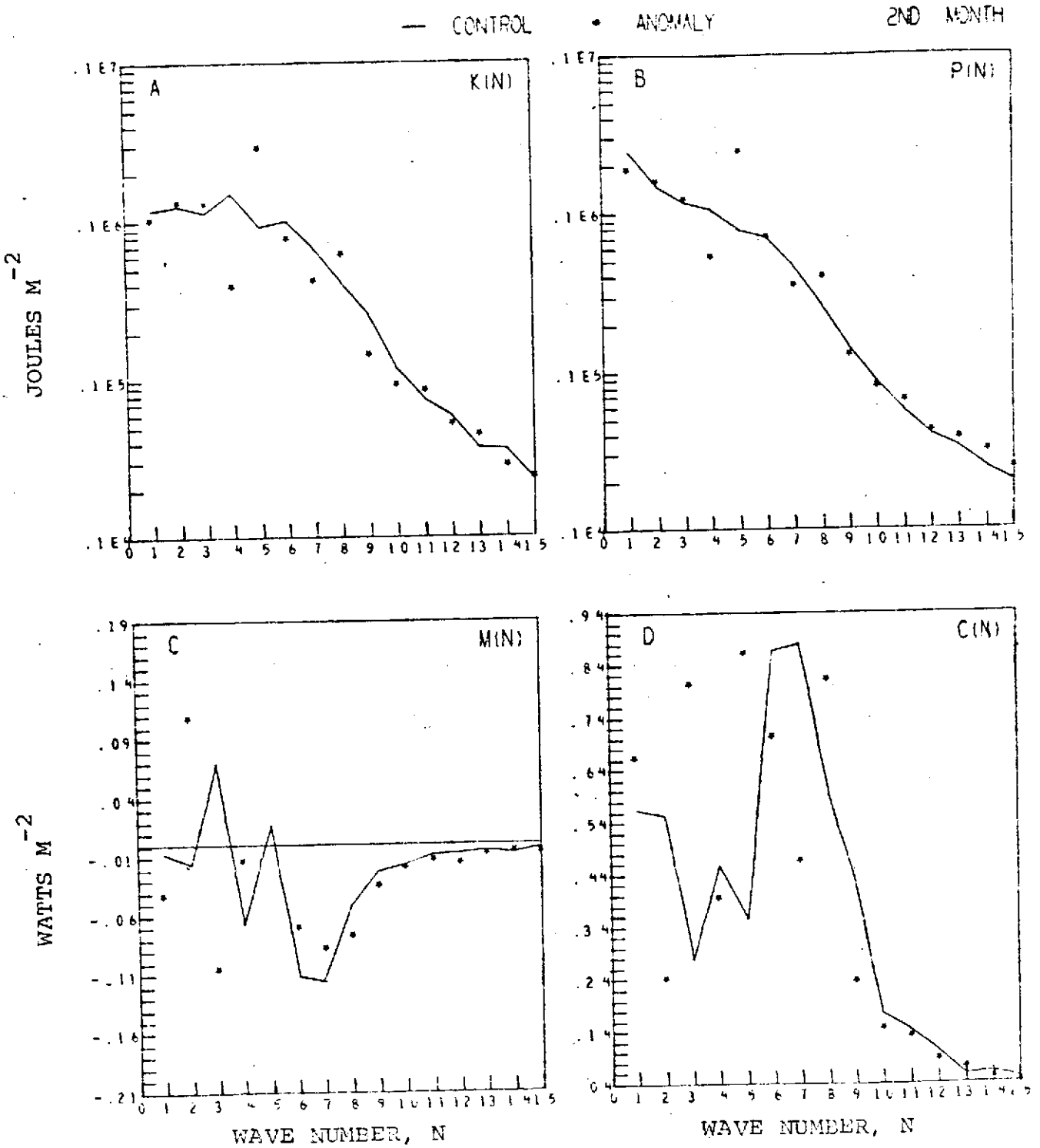

Fig. 21. Same as Fig. 20, for the second month.

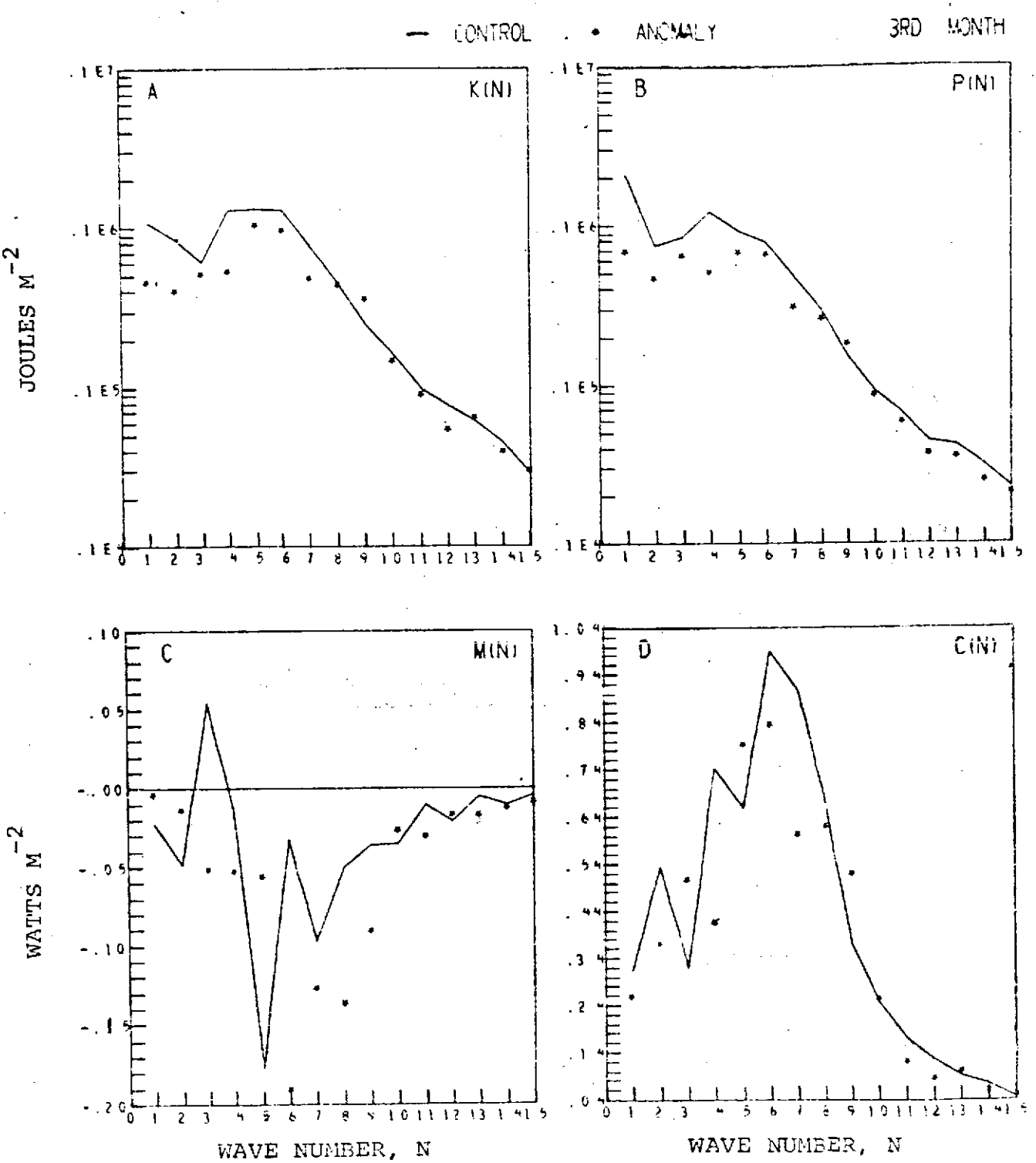

Fig. 22. Same as Fig. 20, for the third month.

$\langle K_Z, P_Z \rangle$ and $\langle K_E, K_Z \rangle$, and the eddy energies in the anomaly run. Fig. 21 illustrates that ultra-long and intermediate waves are fairly disturbed by the SST anomaly. The anomaly appears to increase particularly the eddy activity of wave number 5. For example, K(5), P(5), and C(5) are markedly increased, and M(5) markedly decreased in the anomaly run. Although not shown in the figures, the eddy of wave number 5 was found to transfer more available potential energy to zonal in the anomaly run. This increase contributes much to the reversal in sign of $\langle P_Z, P_E \rangle$ in the southern middle latitudes.

In the third month, the most noteworthy responses to the anomaly in the southern middle latitudes are the reversal in sign of W_E and the large decrease in the eddy energies (Table 4). The anomaly causes W_E in the anomaly run to transport energy out of the southern middle latitudes instead of importing energy into the southern middle latitudes as in the control run. The conversions $\langle P_E, K_E \rangle$ and $\langle P_Z, P_E \rangle$ are also decreased by the transient warm pool. Figs. 22A and 22B illustrate that eddy energies decrease over all waves in the anomaly run. The reduction of eddy conversion also occurs over most of the waves (Fig. 22D). In the anomaly run all waves in the southern middle latitudes were found to be barotropically stable, while the eddy of wave number 3 in the control run is not (Fig. 22C).

In general, the analysis of the regional energetics

both in the spatial and wave-number domains show that the middle latitudes of both hemispheres can indeed exhibit a great response to a transient North Pacific SST anomaly.

8. Conclusions and further remarks

Two aspects of the problem under investigation are (1) the ability of the two-level Mintz-Arakawa model to simulate the atmospheric energetics, and (2) the possible effects of a transient North Pacific SST anomaly on the energetics of the atmosphere. For the first problem, the energetics of the control run, which was designed to simulate normal climate, were compared with the observations. For the second problem, the energetics of the anomaly run, corresponding to a transient anomalous SST pattern, were compared with the control run.

Except in the tropics, the two-level Mintz-Arakawa model exhibits a reasonable and realistic energy budget. For the area north of 20°N, except for the diabatic generation of eddy available potential energy, the energy budgets both in the spatial and wave-number domains show good agreement between the control run and the observations. In the tropics, the convective precipitation was found to have a dominating influence on the model energetics.

One major defect of the model simulation is caused by the parameterization of convection, which produces too much convective precipitation in the tropics. The excessive rainfall is accompanied by the release of too much latent heat of condensation, and hence magnifies the diabatic generation of available potential energy in the tropics. It also increases the vertical velocities which in turn intensify

the conversion from available potential to kinetic energy. These results further affect other atmospheric energy processes in the tropics. Thus, improvement on the parameterization of convection may bring the simulated tropical energetics closer to the reality.

The analysis of the spectral energy budget of the control run for the area north of $20^{\circ}N$ reveals that the spectral components of eddy energies, P(n) and K(n), are generally smaller in the model than in nature, as are the conversions from P_z to P(n). The coarse horizontal resolution in the model might be responsible for these shortcomings. The model was found to produce excessively high temperature in the tropics, presumely due to the excessive convective precipitation in the tropics. This bring about a much larger meridional temperature gradient in middle latitudes in the model. Therefore, the fact that the conversions from P_z to P(n) are too small in the model implies that the eddies are less effective in transporting sensible heat poleward.

In the SST anomaly experiment, the imposed positive anomalous pattern has two immediate effects in the first month. One is to augment the sensible heat transfer from sea to air and the evaporation over the local anomaly region. This in turn increases the released latent heat and hence increases the diabatic generation of eddy available potential energy, G_E. The other is to increase the sea surface temperature gradients, especially on the northern side of the warm pool.

This then increases the baroclinic instability and eddy conversion, C(n), around the intermediate scales. Since the mean motion of the atmosphere is mainly parallel to the latitude circles, and the cyclone paths are toward northeast, these effects spread to the other parts of the northern middle latitudes. These two effects further intensify other eddy activities, e.g., K(n), P(n), Q(n), and M(n), around the intermediate scales in the northern middle latitudes (Fig. 17).

However, an unexpected result in the first month is that the anomaly appears to cause a marked reduction in the eddy activity of the ultra-long waves, especially wave number 2, in the northern middle latitudes (Fig. 17). Because most of the increase of eddy activity around the intermediate scales is compensated by the reduction in ultra-long waves, the net eddy activity shows only a minor increase in the northern middle latitudes (Table 3). Although the first month's gross regional energetics in the spatial domain are slightly affected by the anomaly (see Tables 3 and 4), the spectral energetics in the northern middle latitudes appear to be considerably disturbed by the SST anomaly.

In the second month, with the removal of the anomalous SST pattern, the portion of the atmosphere above the first month's warm pool tends to experience a reduction of surface sensible heat exchange and evaporation. This reduces the condensation and hence decreases G_E. It also

decreases the vertical velocities, and this in turn reduces the eddy conversion $\langle P_E, K_E \rangle$. These effects further affect other energetics and induce significantly large response in the northern middle latitudes. As shown in Table 3, eddy energies, P_E and K_E, and the conversion $\langle P_Z, P_E \rangle$ are also reduced in the anomaly run, and the conversions $\langle K_Z, P_Z \rangle$ and $\langle K_E, K_Z \rangle$, and the eddy pressure interaction, W_E, in the anomaly run are changed in sign as compared with the control run. The reduction in $\langle P_Z, P_E \rangle$ and the weaker indirect cell further imply that the poleward eddy transports of sensible heat and momentum may be reduced by the anomaly. In general, the transient SST anomaly causes a reduction in eddy activity in the northern middle latitudes. The reduced eddy activity was found to take place at all wave numbers, with the major reduction in the longer waves (Fig. 18).

The southern middle latitudes in the second month are also considerably disturbed by the anomaly, e.g., a reversal in sign of $\langle P_Z, P_E \rangle$, and an increase in $\langle K_Z, P_Z \rangle$, $\langle K_E, K_Z \rangle$, P_E, and K_E (Table 4). Longer waves are fairly disturbed by transient warm pool, especially wave number 5 showing a marked increase in eddy activity (Fig. 21).

The global energetics in the third month are still fairly disturbed by the transient SST anomaly. According to Tables 3 and 4 and Figs. 19 and 22, the eddy activity generally increases in northern middle latitudes but decreases in southern middle latitudes, and the variations of eddy

activities take place primarily in the longer waves.

The third month's tropical energetics were found to be severely distorted in the anomaly run compared with the control run (Figs. 5, 6, 12 - 16). This is due primarily to the extremely large reduction of precipitation at 2^{o}S. Due to the unsatisfactory parameterization of convection in the model, this tropical effect is not considered as a true reflection of nature, but rather as a computational artifact caused by a model defect. In order to simulate more reliably the effects of SST anomalies in the tropics, an improvement in the treatment of convection is badly needed. (Note that this improvement was included in Arakawa (1972) 3-layer model, and has been retained in GISS 9-layer model (Somerville et al., 1974)).

Although the anomalous SST pattern persists for only one month, the results indicate that the transient SST variations of reasonable magnitude in the North Pacific Ocean can induce a disturbing effect on the global energetics both in the spatial and wave-number domains. This implies that modest variations in the sea surface temperature may cause a significant change in the monthly or seasonal synoptic patterns over the whole earth, and that a precise knowledge of the time-dependent sea surface temperature field may be important for the long-range weather prediction. It remains to be seen whether this is a property only of the model, or if it is indeed a true reflection of nature.

References

Arakawa, A., 1972: Design of the UCLA atmospheric general circulation model. University of California at Los Angeles, Dept. of Meteorology, Technical Report No. 7.

_____, A. Katayama, and Y. Mintz, 1968: Numerical simulation of the general circulation of the atmosphere. Proceedings of the WMO/IUGG Symposium on Numerical Weather Prediction, Tokyo, IV-7-IV-8-12.

Bjerknes, J., 1966:A possible response of the atmospheric Hadley circulation to equatorial anomalies of ocean temperatures. Tellus, 18, 820-829.

_____,1969: Atmospheric teleconnections from the equatorial Pacific. Mon. Wea. Rev., 97, 163-172.

Brown, J.A., 1964: A diagnostic study of tropospheric diabatic heating and the generation of available potential energy. Tellus, 16, 371-388.

_____, 1967: On atmospheric zonal to eddy kinetic energy excgange for January 1963. Tellus, 19, 14-16.

Brown, J.A., 1969: A numerical investigation of hydrodynamic instability and energy conversions in the quasi-geostropic atmosphere: Part I. J. Atmos. Sci., 26, 352-365.

Charney, J.G., 1947: The dynamics of long waves in a baroclinic westly current. J. Meteor., 4, 135-162.

Dutton, J.A., and D.R. Johnson, 1967: The theory of available potential energy and a variational approach to atmospheric energetics. Adv. Geophys., 12, 333-436.

Gates, W.L., 1972: The January global climate simulated by the two-level Mintz-Arakawa model: A comparsion with observation. Rand Corporation, Santa Monica, California, Report R-1005-ARPA. Nov. 1972, 107 pp.

_____, E.S. Batten, A.B. Kahle, and A.B. Nelson, 1971: A documentation of the Mintz-Arakawa two-level atmospheric general circulation model. Rand Corporation, Santa Monica, California, Report R-877-ARPA. Dec. 1971, 408 pp.

Haltiner, G.J., 1967: The effects of sensible heat exchange on the dynamics of baroclinic wave. Tellus, 19, 183-198.

Holloway, J.L., Jr., and S. Manabe, 1971: Simulation of climate by a global general circulation model: I. Hydrologic cycle and heat balance. Mon. Wea. Rev., 99, 335-370.

Kasahara, A., and W.M., Washington, 1967: NCAR global general circulation model of the atmosphere. Mon. Wea. Rev., 95, 389-402.

Krueger, A.F., J.S. Winston, and D.A. Haines, 1965: Computations of atmospheric energy and its transformation for the northern hemisphere for a recent five-year period. Mon. Wea. Rev., 93, 227-238.

Kung, E.C., 1967: Diurnal and long-term variations of the kinetic energy generation and dissipation for a five-year period. Mon. Wea. Rev., 95, 593-606.

Kuo, H.-L., 1949: Dynamic instability of two-dimensional nondivergent flow in a barotropic atmosphere. J. Meteor., 6, 105-122.

Leith, C.E., 1965: Numerical simulation of the earth's atmosphere. Methods in Computational Physics, 4, 1-28.

Lorenz, E.N., 1955: Available potential energy and the maintenance of general circulation. Tellus, 7, 157-167.

Manabe, S., J. Smagoringsky, J.L. Holloway, Jr., and H.M. Stone, 1970: Simulated climatology of general circulation model with hydrologic cycle: III Effects of increased horizontal computational resolution. Mon. Wea. Rev., 98, 175-212.

_____, J.L. Holloway, Jr., and H.M. Stone, 1971a: Tropical circulation in a time-integration of a global model of the atmosphere. J. Atmos. Sci., 27, 580-613.

Margules, M., 1903: Über die energie der stürme. Jahrb. kaiskön Zent. für Met., Vienna. Translation by C. Abbe in Smithson. Misc. Coll., 51, 1910.

Mintz, Y., 1965: Very long-term global integration of the primitive equations of atmospheric motion: An experiment in climate simulation. WMO Technical Notes No. 66, 141-167.

Mintz, Y., A. Katayama, and A. Arakawa, 1972: Numerical simulation of the seasonally and inter-annually varying tropospheric circulation. Proceedings of the Survey Conference, February 15-16 1972, Climatic Impact Assessment Program, Cambridge, Mass. U. S. Dept. of Transportation, Report No. DOT-TSC-OST-72-13, Sept. 1972, 281 pp.

Murakami, T., and T. Tomatsu, 1965: Energy cycle in the lower troposphere. WMO Technical Notes No. 66, 295-331.

Namias, J., 1963: Large-scale air-sea interaction over the North Pacific from summer 1962 through the subsequent winter. J. Geophys. Res., 68, 6171-6186.

_____, 1969: Seasonal interactions between the North Pacific Ocean and the atmosphere during the 1960's. Mon. Wea. Rev., 97, 173-192.

_____, 1971: The 1968-69 winter as an outgrowth of sea and air coupling during antecedent seasons. J. Phys. Ocean., 1, 65-81.

Oort, A. H., 1964: On estimates of the atmospheric energy cycle. Mon. Wea. Rev., 92, 483-493.

Saltzman, B., 1957: Equations governing the energetics of the larger scales of atmospheric turbulence in the domain of wave number. J. Meteor., 14, 513-523.

_____, 1970: Large-scale atmospheric energetics in the wave number domain. Rev. Geophys. Space Phys., 8, 289-302.

_____, and A. Fleisher, 1960: The modes of release of available potential energy in the atmosphere. J. Geophys. Res., 65, 1215-1222.

_____, 1961: Further statistics on the modes of release of available potential energy. J. Geophys. Res., 66, 2271-2273.

Smagorinsky, J., 1953: The dynamical influence of large-scale heat sources and sinks on the quasi-stationary mean motions of the atmosphere. Quart. J. Roy. Meteor. Soc., 97, 342-366.

Smagorinsky, J., S. Manabe, and J.L. Holloway, Jr., 1965: Numerical results from a nine-level general circulation model of the atmosphere. Mon. Wea. Rev., 93, 727-768.

Somerville, R.C.J., P.H. Stone, M. Halem, J.E. Hansen, J.S. Hogan, L.M. Druyan, G. Russell, A.A. Lacis, W.J. Quirk, and J. Tenenbaum, 1974: The GISS model of the global atmosphere. J. Atmos. Sci., 31, 84-117.

Spar, J., 1973a: Some effects of surface anomalies in a global general circulation model. Mon. Wea. Rev., 101, 91-100.

_____, 1973b: Transequatorial effects of sea surface temperature anomalies in a global general circulation model. Mon. Wea. Rev., 101, 554-563.

_____, 1973c: Supplementary notes on sea-surface temperature anomalies and model-generated meteorological histories. Mon. Wea. Rev., 101, 767-773.

Starr, V.P., and J.M. Wallace, 1964: Mechanics of eddy processes in the tropical troposphere. Pure Appl. Geophys., 58, 138-144.

Van Mieghem, J., 1956: The energy available in the atmosphere for conversion into kinetic energy. Beitr. Phys. Fr. Atmos., 29, 129.

Vincent, D.G., 1969: Seasonal changes in the global atmospheric energy balance and results for restricted regions. Ph. D. dissertation, Massachusetts Institute of Technology, 173 pp.

Wellck, R.E., A. Kasahara, W.M. Washington, and G. Santo, 1971: Effect of horizontal resolution in a finite-difference model of the general circulation. Mon. Wea. Rev., 99, 673-683.

Wiin-Nielsen, A., and J.A. Brown, 1960: On diagnostic computations of atmospheric heat sources and sinks and the generation of available potential energy. Proceedings of the International Symposium on Numerical Weather Prediction, Tokyo, 1960, Meteor. Soc. Japan, Mar. 1962, 593-613.

_____, and M. Drake, 1964: Further studies of energy exchange between the zonal flow and the eddies. Tellus, 16, 168-180.

Yang, C.-H., 1967: Nonlinear aspects of the large-scale motion in the atmosphere. University of Michigan, Technical Report 08759-1-T, 173 pp.